Hindawi
Shock and Vibration
Volume 2021, Article ID 8830841, 25 pages
https://doi.org/10.1155/2021/8830841

Research Article

Motion Control of a 4WS4WD Path-Following Vehicle: Further Studies on Steering and Driving Models

Zhonghua Zhang,[1] **Caijin Yang**,[1] **Weihua Zhang**,[1] **Yanhai Xu**,[2] **Yiqiang Peng**,[2] **and Maoru Chi**[1]

[1]*State Key Laboratory of Traction Power, Southwest Jiaotong University, Chengdu 610031, China*
[2]*School of Transportation and Automotive Engineering, Xihua University, Chengdu 610039, China*

Correspondence should be addressed to Caijin Yang; ycj78_2012@163.com

Received 10 June 2020; Revised 22 November 2020; Accepted 19 December 2020; Published 6 January 2021

Academic Editor: Gang Tang

Further research on motion control of a 4WS4WD path-following vehicle is carried out in this paper. Focuses are placed on understanding and testing the vehicle path-following control models developed previously at a deep level. Control models are in relation to parameters introduced, and the effects of these parameters are discovered. Control models are interpreted by dynamic simulation using a 3DOF vehicle model with three cases. Three kinds of planned paths are considered in these cases to test control performances, which include the straight, circular, and sinusoidal paths. Interesting dynamic results are obtained and analyzed qualitatively, e.g., various steering modes. Simulation studies are extended with consideration of a fine vehicle dynamic model established in CarSim and a complex path composed of straight and curved segments. Control models are examined in a complex problem, and results obtained show that they are validated with robustness in dynamic environment.

1. Introduction

Due to outstanding maneuvering and acceleration performances, the 4WS4WD vehicles [1, 2] have been received attentions from researchers and engineers in recent years. Major concerns are motion controls of these overactuated vehicles, e.g., lateral stability control [3–7] and autonomous path-following control [8–23]. Vehicle lateral control systems can help the drivers to change the lanes safely or assist them in performing evasive maneuvers. Effective lateral control algorithms were developed in previous literatures [3–7]. Liang et al. [3] proposed a comprehensive control method for 4WID4WIS vehicles, which integrated active steering (AS) and direct yaw moment control (DYC) systems. In Ref. [3], the decoupling control method and penalty function were used to allocate the involvement of AS and DYC for the vehicle in the case of a slight or moderate steering. For a large steering, the handling-oriented and stability-oriented control approaches were proposed based on sideslip phase plane, which accounted for a fine trade-off between the handling and stability performances of the vehicle. In order to tack the desired lateral velocity and yaw rate, Hu et al. [4] studied a novel integrated optimal dynamics controller for the 4WS4WD electric vehicles by using hierarchical control methodology. The controller was based on the LQR-method and developed in the high-lever design. As the controller was used in the low-level design, control signals were allocated through a cost function to generate optimal tire forces. In Ref. [5], a control coordination system for 4WID4WIS vehicles was proposed based on linear quadratic regulator and fuzzy logic. This system was composed of a PID controller for tracking the desired vehicle steering and a sliding mode control controller for power-assisted steering. Xiong et al. [6] designed a vehicle dynamic control system for a four in-wheel motor drive electric vehicle with consideration of tire cornering stiffness estimation and the vehicle stability under critical driving conditions. Li et al. [7] presented an adaptive SMC control scheme to improve handling and stability of electric vehicles equipped with four in-wheel motors.

With the demand for autodriving techniques in automotive industry, the path-following control design for 4WS4WD vehicles becomes an interesting but challenging research topic. Early relevant studies were concerned with 4WS4WD mobile robots, which were based on the kinematics models without dynamic effects and under the assumption that the wheeled robot operated at low speeds and low accelerations [8–10]. Later on, researchers resumed the vehicle path-following problem [11–23] using various control methods, e.g., the proportional-integral-derivative (PID), model predictive control (MPC), fault tolerant control (FTC), and convex optimization. Dai and Katupitiya [11] designed the driving controller and steering controller for the 4WS4WD vehicles in the PID law. The controllers were validated by dynamic simulation at a low velocity level of 3 m/s. Simulation results showed that the controllers took effect in the presence of uncertainties. The PID control law was adapted in Ref. [12] by combining neural networks and electronic differential laws. An improved control strategy was thus proposed to determine target speeds of four in-wheel motors. Simulation on controls in Ref. [12] were performed in the cases of the vehicle velocities 10 km/h and 15 km/h. Xiao et al. [13] considered the cornering cutting problem and built a fuzzy controller with good tracking accuracy. In the controller, the look-ahead distance was dynamically adjusted according to the curvature of the target trajectory. Bian et al. [14] designed a Takagi–Sugeno fuzzy model predictive controller for four wheels steering and four wheels driving electric vehicles. This controller combined lane keeping and speed tracking of the vehicle. Peng [15] introduced a novel idea for controlling wheel torque and wheel steering. The key of the idea was in that the original constrained tracking problem was transformed to the vehicle state regulation. In control implement, an integral compensation with low-and-high gain technique was exploited to simultaneously eliminate steady-state error of the path-following and enhance utilization of the constrained wheel slip. In order to evaluate optimal driving forces and steering angles, Tan et al. [16] designed a close-loop path-following control system of 4WS4WD vehicles. The control strategy was achieved with the combination of MPC and allocation. Control inputs were calculated by an online sequential quadratic programming optimization method. Schwartz et al. [17] developed a model predictive control allocation algorithm for overactuated electric vehicles with individually steered and driven wheels. In the control design, the tire dynamics, actuator dynamics, and constraints on state variables, as well as input and output variables, were taken into account. A nonlinear model predictive control problem was presented, which was normalized and transferred into the discrete-time domain with the forward Euler method.

Considering the overactuated properties, some researchers attempted to use the online optimization methods [18–20] to study the path-following control of 4WS4WD vehicles. Dai and Katupitiya [18, 19] integrated the sliding mode control and particle swarm optimization and proposed a novel path-following control method. This method was based on a vehicle kinematics model and could achieve good path-following performance. An SMC-based steering controller was used to eliminate the offset and heading errors with respect to the reference path. Four driving forces of the vehicle were optimized by PSO in real time. The control method was examined in simulation under low vehicle velocities of 3 m/s and 4 m/s. By contrast, Ono et al. [20] based on vehicle dynamics proposed an integrated control algorithm using an online-nonlinear optimization method for the 4WS4WD vehicles, which could minimize the working load of each tire.

Besides the above motion control methods for 4WS4WD vehicles, the path-following performances of the vehicle under fault conditions were worthy of being investigated. The in-wheel motor can fail by mechanical failures, overheat, or motor driver faults. Considering the faults of motors, some researchers designed the fault-tolerant path-following control system [21–23] for 4WS4WD vehicles. Zhang and Cocquempot [21] proposed a passive fault tolerant control scheme to achieve the vehicle stability and path-following performance in faulty situations. In the controller design, a simple and active fault diagnosis approach was used. A fault tolerant lateral control strategy was implemented in presence of unknown component faults, which was based on flatness theory and the back-stepping technique. Dynamic simulation showed that the proposed control algorithm was effective under fault conditions. In Ref. [22], the output tracking control problem for 4WS4WD vehicles was formulated in the presence of significant model uncertainties. An adaptive fault tolerant control (FTC) scheme was designed. Numerical simulations were performed for validation purpose. Haddad et al. [23] also presented a fault tolerant control strategy for maintaining the lateral stability of a 4WS4WD autonomous vehicle in presence of an unknown component fault.

Despite that great efforts were made and achievements were obtained in early works [8–23], the 4WS4WD vehicle needs to be studied in many aspects, especially in developing a fast, effective, and robust path-following control method. For this purpose, a potential method was developed to determinate steering angles and driving forces of wheels for achieving accurate path-following of the vehicle in previous research of the authors. This paper presents further studies on steering and driving control models developed previously. Effects of parameters in control models are discovered firstly. The path-following dynamic analysis is then carried out to understand control models by a 3DOF nonlinear vehicle model. Typical straight and circular trajectories are considered as planned paths in the analysis. In addition, a sinusoidal trajectory is also included. Interesting results are obtained and qualitatively analyzed. The analysis is finally extended with consideration of a fine vehicle model established in CarSim and a complex planned path. Control models are validated in complex situations and can maintain good robust performance. Original contributions of this paper are summarized as follows. (1) Steering and driving control models are understood in various aspects. In control design, a dynamical self-adaptive trajectory of the vehicle is generated once control parameters are given, which is based on vehicle states and stably converges to the planned path. It is the key of the controller. This finding is attractive and

significant. For example, it can be applied to real time navigation and obstacle avoidance for autonomous ground vehicles (AGVs) in dynamic environment. (2) Interesting results are obtained and analyzed. Control parameters have active effects on the path-following accuracy of the vehicle controlled. Moreover, control models allocate multiple steering modes, which largely depend on initial and dynamic states of the vehicle. (3) Control models are examined in a complex path-following problem and validated with robustness in dynamic environment.

2. Theoretical Fundamentals

Though focuses are placed on further studying control models developed, relevant details are briefly provided here for completeness of this paper, including dynamic model of the vehicle, path-following dynamics of the vehicle, and determination of steering and driving control variables.

2.1. Vehicle Dynamic Model. A classical single track model [3, 14, 18] is used to describe the vehicle dynamics, as shown in Figure 1. For the sake of simplicity, the interaction between longitudinal tire force and lateral tire force is ignored, which is treated as external disturbance in the steering and driving control model. Considering the limit of tire longitudinal force is approximately proportional to the tire vertical load [24], the longitudinal force F_l^f of the front wheel is assumed to be a proportional relationship of the longitudinal force F_l^r of the rear wheel by vertical load distribution coefficient k_l. Taking into account the lower costs, ignoring the effect of accelerating and decelerating, the k_l is a constant and equal to the ratio of distances from mass center of the vehicle to rear and front axles. Let δ_f and δr be steering angles of front and rear wheels. The vehicle has mass m and inertia moment J. The position of mass center of the vehicle is represented by X_C and Y_C, which are defined in a global inertial coordinate system. θ is the yaw angle of the vehicle.

The dynamic model of the vehicle can be described as

$$\mathbf{M}\ddot{X} = \mathbf{F}\left(\delta_f, \delta_r, F_l^f, F_l^r\right), \tag{1}$$

where the coordinate vector **X**, the mass matrix **M**, and the force vector **F** are, respectively,

$$\mathbf{X} = \left[X_C, Y_C, \theta\right]^T, \tag{2}$$

$$\mathbf{M} = \begin{bmatrix} m & 0 & 0 \\ 0 & m & 0 \\ 0 & 0 & J \end{bmatrix}, \tag{3}$$

$$\mathbf{F} = \begin{bmatrix} f_x\left(\delta_f, \delta_r, F_l^f, F_l^r\right)\cos\theta - f_y\left(\delta_f, \delta_r, F_l^f, F_l^r\right)\sin\theta \\ f_x\left(\delta_f, \delta_r, F_l^f, F_l^r\right)\sin\theta + f_y\left(\delta_f, \delta_r, F_l^f, F_l^r\right)\cos\theta \\ M_z\left(\delta_f, \delta_r, F_l^f, F_l^r\right) \end{bmatrix}, \tag{4}$$

in which the forces f_x and f_y and the moment M_z are given in Appendix A of this paper.

2.2. Path-Following Dynamics. A moving vehicle may deviate from the path due to road disturbances. The unexpected states of the vehicle can be described using the lateral deviation ε_d and the heading deviation ε_θ, as illustrated in Figure 1. The lateral deviation ε_d is defined as a minimal distance from a control point in the vehicle to the planned path. The heading deviation ε_θ actually represents the angle between the vehicle and the reference road. In addition, the vehicle is always expected to run at given velocities. The velocity deviation ε_v is considered here for an accurate path-following description. The velocity deviation ε_v is a difference between the instantaneous and planned velocities of the vehicle in the longitudinal direction.

Without of loss generality, the vehicle path-following is essentially a dynamic process that three deviations converge to zeros and remain constantly. Hence, the path-following process of the vehicle can be described as follows:

$$\ddot{\varepsilon}_d + c_d\dot{\varepsilon}_d + k_d\varepsilon_d = 0, \tag{5}$$

$$\ddot{\varepsilon}_\theta + c_\theta\dot{\varepsilon}_\theta + k_\theta\varepsilon_\theta = 0, \tag{6}$$

$$\dot{\varepsilon}_v + c_v\varepsilon_v = 0, \tag{7}$$

where c_d, k_d, c_θ, k_θ, and c_v are control parameters introduced. Clearly, deviations in equations (5)–(7) absolutely converge to zeros in terms of ordinary differential equation theory. For a certain path defined by the equation $\varphi(X, Y) = 0$, three deviations ε_d, ε_θ, and ε_v can be explicitly expressed in coordinates X_C, Y_C, and θ. They are as follows:

$$\varepsilon_d = f_d\left(X_C, Y_C, \theta\right) = \sqrt{\left(X_C - X_P\right)^2 + \left(Y_C - Y_P\right)^2}, \tag{8}$$

$$\varepsilon_\theta = f_\theta\left(X_C, Y_C, \theta\right) = \cos^{-1}\left(\mathbf{h}^T\mathbf{n}_\tau\right), \tag{9}$$

$$\varepsilon_v = f_v\left(\dot{X}_C, \dot{Y}_C, \theta, t\right) = V_d - V_t = \dot{X}_C\cos\theta + \dot{Y}_C\sin\theta - V_t, \tag{10}$$

where X_P and Y_P are position coordinates of projection point of vehicle mass center on the path, V_d and V_t are the instantaneous and planned velocities of the vehicle in the longitudinal direction, as shown in Figure 1, and the unit tangent direction $\mathbf{n}_\tau$ of the path at projection point and the unit heading direction **h** of the vehicle are, respectively, defined by

$$\mathbf{n}_\tau = \frac{1}{\sqrt{\varphi_X^2 + \varphi_Y^2}}\left[-\varphi_Y, \varphi_X\right]^T, \qquad \mathbf{h} = \left[\cos\theta, \sin\theta\right]^T. \tag{11}$$

Considering equations (8)–(10), equations (5)–(7) can be rewritten as

$$\overline{M}\ddot{X} = \overline{F}, \tag{12}$$

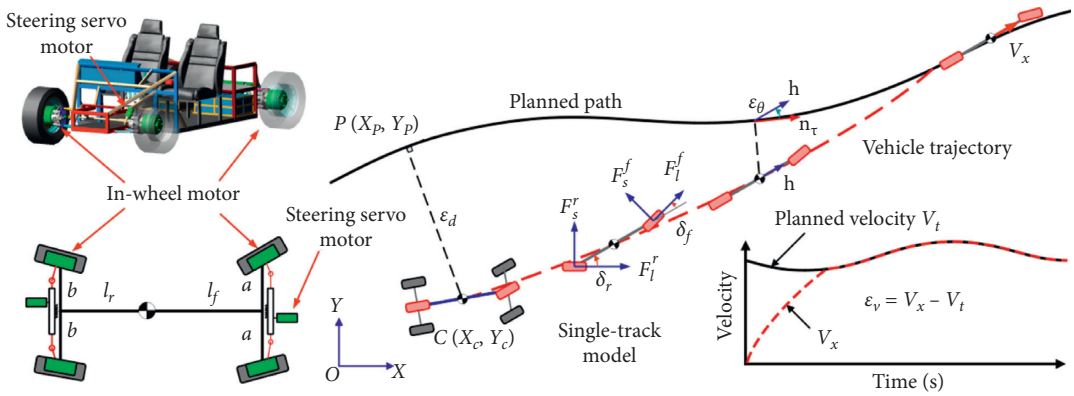

FIGURE 1: Schematic of a 4WS4WD vehicle system.

where the three by three matrix $\overline{M}$ and the vector $\overline{F}$ are given in Appendix A.

2.3. Control Models. There are four control variables in controller design for the vehicle system shown in Figure 1. With considering the assumption condition stated above,

$$F_l^f = k_l F_l^r. \tag{13}$$

Three independent control variables required are then driving force F_l^r and steering angles δ_f and δ_r. Now, these control variables are determined from equations (1) and (12). For this purpose, equation (1) is transformed to

$$\ddot{X} = \mathbf{M}^{-1}\mathbf{F}, \tag{14}$$

and substituting equation (14) into equation(12) leads to

$$\mathbf{F}\left(F_l^r, \delta_f, \delta_r\right) = \overline{M}^{-1}\mathbf{M}\overline{F}. \tag{15}$$

The approximation of equation (15) yields

$$\mathbf{Ax} = \mathbf{b}, \tag{16}$$

where $\mathbf{x} = [F_l^r, \delta_f, \delta_r]^T$ is the vector of control variables, and the matrix $\mathbf{A}$ and the vector $\mathbf{b}$ are given in Appendix A. Thus, steering and driving control models are addressed in equation (16). Without loss of generality, parameters and variables in equation (16) are known or measurable. In that sense, equation (16) is solvable. However, it is not an easy task because equation (16) is complex. A feasible technique is adopted to solve equation (16) for determining control variables, which is presented in the following section.

3. Implementations

Steering and driving control models for a 4WS4WD path-following vehicle in this paper are briefly presented above. In this section, control models are discussed in application aspect. For an easy use, they are simplified in two cases that the vehicle follows the straight and circular paths. Their application in dynamic simulation is introduced subsequently. Important details are provided below.

3.1. Reduction of Control Models. It is remarkably noted that control models are derived with consideration of a general path. Control models are thus addressed in an implicit form and sometimes complex. Since an actual path in engineering application is often composed of straight and circular segments, the realization of control models in these two cases is emphatically discussed here.

As the vehicle follows a straight path characterized by gradient k and intercept b, relevant deviations can be approximated as follows:

$$\varepsilon_d \approx Y_C - kX_C - b, \tag{17}$$

$$\varepsilon_\theta \approx \sin\theta - k\cos\theta. \tag{18}$$

Considering equations (17), (18), and (10) and performing the derivations as above, corresponding formulas are then obtained as follows:

$$\overline{M} = \begin{bmatrix} -k & 1 & 0 \\ \cos\theta & \sin\theta & 0 \\ 0 & 0 & k\sin\theta + \cos\theta \end{bmatrix},$$

$$\overline{F} = \begin{bmatrix} -c_d\left(\dot{Y}_C - k\dot{X}_C\right) - k_d\left(Y_C - kX_C - b\right) \\ \left(\dot{X}_C\sin\theta - \dot{Y}_C\cos\theta\right)\dot{\theta} + \dot{V}_t - c_v\left(\dot{X}_C\cos\theta + \dot{Y}_C\sin\theta - V_t\right) \\ -(k\cos\theta - \sin\theta)\dot{\theta}^2 - c_\theta(k\sin\theta + \cos\theta)\dot{\theta} - k_\theta(\sin\theta - k\cos\theta) \end{bmatrix}. \tag{19}$$

Similarly, as the vehicle follows a circular path characterized by the center (X_0, Y_0) and radius R, main formulas are given as follows:

$$\varepsilon_d \approx (X_C - X_0)^2 + (Y_C - Y_0)^2 - R^2,$$

$$\varepsilon_\theta \approx (X_C - X_0)\cos\theta + (Y_C - Y_0)\sin\theta,$$

$$\overline{M} = \begin{bmatrix} X_C - X_0 & Y_C - Y_0 & 0 \\ \cos\theta & \sin\theta & -(X_C - X_0)\sin\theta + (Y_C - Y_0)\cos\theta \\ \cos\theta & \sin\theta & 0 \end{bmatrix},$$

$$\overline{F} = \begin{bmatrix} -\dot{X}_C^2 - \dot{Y}_C^2 - c_d \begin{pmatrix} (X_C - X_0)\dot{X}_C + \\ (Y_C - Y_0)\dot{Y}_C \end{pmatrix} - \frac{1}{2}k_d \begin{pmatrix} (X_C - X_0)^2 + \\ (Y_C - Y_0)^2 - R^2 \end{pmatrix} \\ 2\dot{X}_C \sin\theta\dot{\theta} - 2\dot{Y}_C \cos\theta\dot{\theta} + (X_C - X_0)\cos\theta\dot{\theta}^2 + (Y_C - Y_0)\sin\theta\dot{\theta}^2 \\ -c_\theta\left(\dot{X}_C \cos\theta + \dot{Y}_C \sin\theta - (X_C - X_0)\sin\theta\dot{\theta} + (Y_C - Y_0)\cos\theta\dot{\theta}\right) - k_\theta\left((X_C - X_0)\cos\theta + (Y_C - Y_0)\sin\theta\right) \\ \left(\dot{X}_C \sin\theta - \dot{Y}_C \cos\theta\right)\dot{\theta} + \dot{V}_t - c_v\left(\dot{X}_C \cos\theta + \dot{Y}_C \sin\theta - V_t\right) \end{bmatrix}. \tag{20}$$

3.2. Realization in Dynamic Simulation. As stated above, control models are addressed in equation (15). Unfortunately, it is highly nonlinear because matrix **A** is also in relation to control variables, which may lead to complex computations and even the failure in solution. In what follows an approximate technique is adopted to solve it. In simulation, numerical integral is always processed at discrete-time steps. For small time steps, there can have

$$\begin{aligned} \cos\delta_f^k &\approx \cos\delta_f^{k-1}, \\ \sin\delta_f^k &\approx \sin\delta_f^{k-1}, \end{aligned} \tag{21}$$

$$\begin{aligned} \cos\delta_r^k &\approx \cos\delta_r^{k-1}, \\ \sin\delta_r^k &\approx \sin\delta_r^{k-1}, \end{aligned} \tag{22}$$

where δ_f^{k-1}, δ_r^{k-1}, δ_f^k, and δ_r^{k-1} are steering angles δ_f and δ_r of front and rear wheels at the k-1th and kth time steps. Remarkably note that similar definitions in equations (21) and (22) are taken for other variables if necessary. Thus, the matrix **A** in equation (15) at the kth time step can be approximated as follows:

$$\mathbf{A}^k = \begin{bmatrix} \begin{pmatrix} k_l \cos\theta^k \cos\delta_f^{k-1} - k_l \sin\theta^k \sin\delta_f^{k-1} \\ +\cos\theta^k \cos\delta_r^{k-1} - \sin\theta^k \sin\delta_r^{k-1} \end{pmatrix} & \begin{pmatrix} \cos\theta^k \sin\delta_f^{k-1} \\ +\sin\theta^k \cos\delta_f^{k-1} \end{pmatrix} C_\alpha^f & \begin{pmatrix} \cos\theta^k \sin\delta_r^{k-1} \\ +\sin\theta^k \cos\delta_r^{k-1} \end{pmatrix} C_\alpha^r \\ \begin{pmatrix} k_l \sin\theta^k \cos\delta_f^{k-1} + k_l \cos\theta^k \sin\delta_f^{k-1} \\ +\sin\theta^k \cos\delta_r^{k-1} + \cos\theta^k \sin\delta_r^{k-1} \end{pmatrix} & \begin{pmatrix} \sin\theta^k \sin\delta_f^{k-1} \\ -\cos\theta^k \cos\delta_f^{k-1} \end{pmatrix} C_\alpha^f & \begin{pmatrix} \sin\theta^k \sin\delta_r^{k-1} \\ -\cos\theta^k \cos\delta_r^{k-1} \end{pmatrix} C_\alpha^r \\ l_f k_l \sin\delta_f^{k-1} - l_r \sin\delta_r^{k-1} & -l_f C_\alpha^f \cos\delta_f^{k-1} & l_r C_\alpha^r \cos\delta_r^{k-1} \end{bmatrix}, \tag{23}$$

where C_α^f and C_α^r are cornering stiffness of front and rear tires and l_f and l_r are the distances from the mass center of the vehicle to the front and rear axles. Once the matrix **A** is numerically calculated in equation (23), control variables are determined at kth time step in a linear way as follows:

$$\mathbf{x}^k = \left(\mathbf{A}^k\right)^{-1}\mathbf{b}^k. \tag{24}$$

After control variables are determined at current time step, the integration may continue for the next time step and the vehicle responses are predicted by means of some algorithms, e.g., an explicit RK45 method used in this paper. A computational process for dynamic simulation is illustrated in Figure 2.

4. Understanding Parameters in Control Models

The effects of parameters introduced in control models are discussed here since control models are in relation to them. As derived above, control models in equation (16) result from the vehicle dynamic model in equation (1) and the path-following dynamics of the vehicle in equation (12). In that sense, control models can capture main dynamic properties of both vehicle dynamics and path-following dynamics of the vehicle. Note that the path-following dynamics of the vehicle are described in three ordinary differential equations of control parameters; see equations (5)–(7) or equation (12) rewritten in a matrix form for these equations. Equation (12) is now numerically studied under given parameters. Some results are shown in Figures 3 and 4.

Figure 3 shows the trajectories of X_C and Y_C govern by equation (12) with consideration of a straight reference path and various control parameters. As observed in Figure 3, there is a dynamic regulation for coordinates X_C and Y_C converging to the reference path. The regulation obviously associates with control parameters. It is concluded in Figure 3 that a certain trajectory can be planned under proper control parameters. This conclusion is very useful. Control models can be understood in this sense that a path is planned in a dynamic environment and then followed by the vehicle controlled. It is the key of the control method in this paper. It can also be applied to real time navigation and obstacle avoidance for the AGV in dynamic environment due to this property. Moreover, the trajectory is mainly in relation to control parameters c_d and k_d. As a circular path is referred, similar results are obtained and shown in Figure 4. Figure 4 shows the trajectories of X_C and Y_C govern by equation (12) with consideration of a circular reference path and various control parameters.

5. Dynamic Results with a 3DOF Vehicle Model

Control models are examined by dynamic simulation. For a qualitative analysis purpose, a classical 3DOF vehicle model is used. In the analysis, the vehicle follows planned paths, including straight, circular, and sinusoidal paths, as well as a compound path. Dynamic results are obtained and analyzed below. In numerical simulation, main parameters of the vehicle model are listed in Table 1.

5.1. Case 1: Straight Path. As the first case, the vehicle follows a straight path. The path is parameterized by the gradient $k = 1$ and the intercept $b = 1$. The vehicle is initially at rest and deviates from the path by $\varepsilon_d = 2$ m and $\varepsilon_\theta = -5$ degree. Initial simulation conditions of (2.83, 1.0, −5.0, 0, 0, 0) are thus calculated. The vehicle in motion has a variable longitudinal velocity, which is given as

$$V_t(t) = \begin{cases} 2t, & t < T_1, \\ 10, & T_1 \le t < T_2, \\ 10 - t, & T_2 \le t < T_3, \\ 5, & T_3 \le t, \end{cases} \tag{25}$$

where time constants T_1, T_2, and T_3 are equal to 5 s, 20 s, and 25 s, respectively. Note that the longitudinal velocity V_t in equation (25) has an unit of m/s.

Motions of the vehicle controlled are simulated for time $t = 30$ s. In simulation, control parameters $c_d = 1.0$, $k_d = 0.15$, $c_\theta = 5$, $k_\theta = 2.5$, and $c_v = 1.0$ are used. Main results are given below. Comparisons of the vehicle trajectory with the planned path are shown in Figure 5(a). As shown in Figure 5(a), the trajectory of the vehicle controlled converges to the planned path successfully. It is obvious that the vehicle follows the planned path, as expected. This fact can be also illustrated quantitatively (see Figures 5(b)–5(d)). Though there is a slight difference between the simulation velocity and the desired velocity of the vehicle, the lateral and heading deviations of the vehicle are better controlled after about time $t = 20$ s, as shown in Figures 5(b)–5(d). In that sense, control models do take effects.

It can be inferred from the curves plotted in Figure 6 that all wheels of the vehicle may turn properly. Steering angles of the vehicle wheels are analyzed. Figure 6 shows the variations of steering angles of four wheels of the vehicle in the time domain. The vehicle is initially on the right side of the path. It needs to turn left so that it can return to the planned path. In this sense, control models should yield positive steering angles of wheels. As shown in Figure 6, the front and rear wheels steer left (corresponding to positive steering angles) relative to the trajectory of the vehicle. In the path-following motion, steering angles of front wheels firstly increase up to a maximum of about 7.5 degree and then decrease to nearly zero values as the vehicle accurately follows the straight path. A similar variation tendency is found in the steering angle curves for rear wheels. Remarkably note that the steering angles of front wheels of the vehicle are always larger than those of rear wheels of the vehicle. It means that the front wheels act on dominantly in the turning.

The velocity and acceleration analysis of the vehicle is carried out. According to equation (25), the longitudinal velocity of the vehicle linearly varies in time with constant accelerations of 2 m/s^2 and −1 m/s^2 in stages I and III, while remains two constants of 36 km/h and 18 km/h in the other two stages. Figures 7(a) and 7(b), respectively, show time domain responses of the velocity and acceleration of mass center of the vehicle in longitudinal and lateral directions. Good agreement of numerical results for the vehicle velocity and acceleration with their analytical solutions is shown. Meanwhile, it can be seen in Figures 7(a) and 7(b) that the lateral motion of the vehicle is controlled better in a short

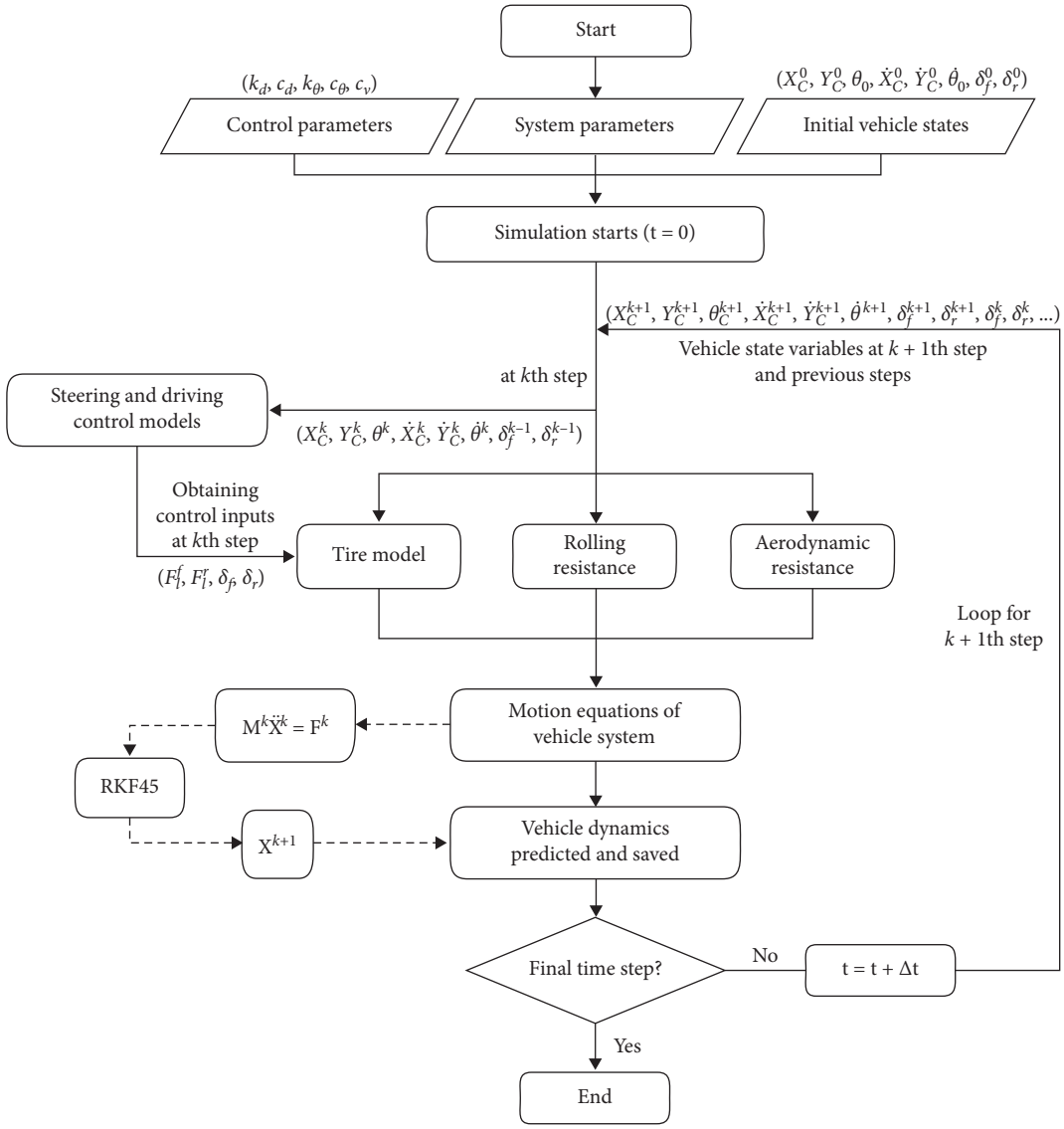

Figure 2: Computational flow diagram of the path-following simulation of the vehicle.

time. In addition, the yaw motion of the vehicle is also controlled (see Figures 7(c)–7(e)). Curves plotted in Figure 7 show that control models do well in presence of coupled motions of the vehicle for the straight path-following motion.

Effects of control parameters k_d and c_d on the path-following dynamics of the vehicle are discussed here. The parameters k_d and c_d have an active influence on the lateral deviation of the vehicle (see Figure 8). As shown in Figure 8, the vehicle has the stable lateral deviation of about zero against with different k_d and c_d. However, the convergence rate of the lateral deviation becomes fast with the increase in k_d or the decrease in c_d. As the vehicle stably follows the straight path, steering angles of all wheels are zeros. Control models address main dynamics of the vehicle in the straight path-following motion.

To further examine control models in the straight path-following motion, simulations are performed with consideration of different path gradients and intercepts, as well as initial states of the vehicle. Simulation results are shown in Figure 9. It can be concluded from Figure 9 that control models are valid in a wide domain.

5.2. Case 2: Circular Path. In this case, the vehicle is controlled to follow a circular path with a radius of $R = 20$ m. The center of the path is at point C (25 m, 25 m). The vehicle starts from initial positions (25 m, 8 m) and the orientation (5 degree) and moves to the planned path with the non-uniform longitudinal velocities. The longitudinal velocity of the vehicle increases from zero to 36 km/h with a constant acceleration of 2 m/s^2 in the first 5 seconds and then remains invariant in a time period of 15 seconds. At time $t = 20$ s, it decreases in a linear way and attains to 18 km/h in 5 seconds. After time $t = 25$ s, it is the constant of 18 km/h. In simulation, control parameters $c_d = 1.6$, $k_d = 0.8$, $c\theta = 8.0$, $k\theta = 5.0$, and $c_v = 0.5$ are used.

Figure 10(a) shows the trajectory of the vehicle controlled in the circular path-following motion. Figures 10(b)–

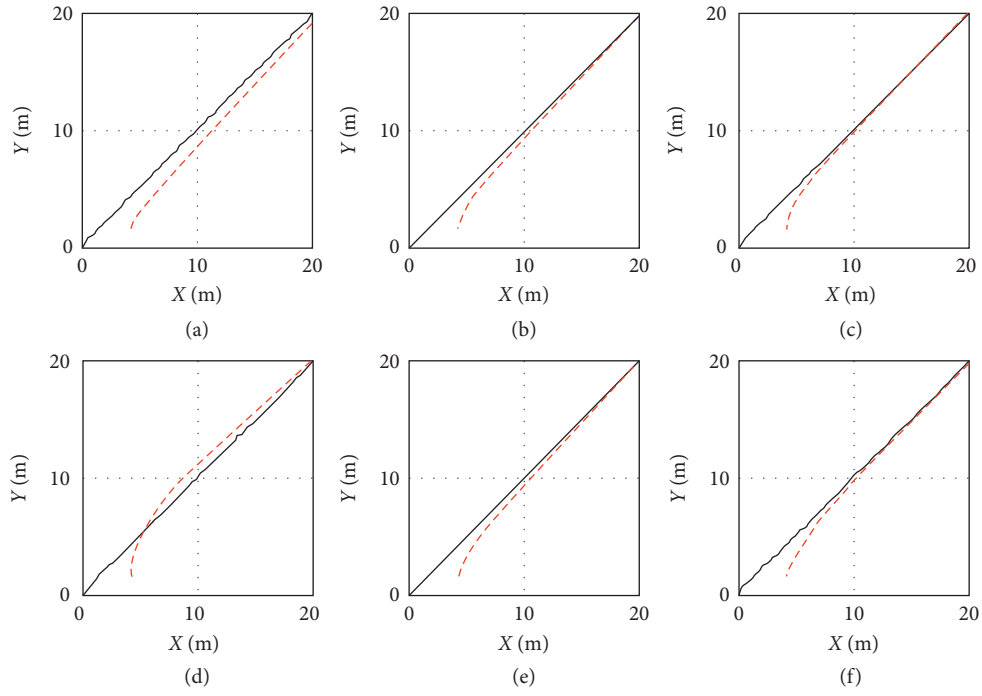

	c_d	k_d	c_θ	k_θ	c_v
(a)	4.0	1.0	2.0	1.0	1.0
(b)	2.0	1.0	2.0	1.0	1.0
(c)	1.4	1.0	2.0	1.0	1.0
(d)	0.5	1.0	2.0	1.0	1.0
(e)	2.0	1.0	1.4	1.0	1.0
(f)	2.0	1.0	0.5	1.0	1.0

FIGURE 3: The trajectories of coordinates X_C and Y_C govern by equation (12) with a straight reference path and various control parameters introduced.

10(d) show the variations of three deviations of the vehicle following the circular path in the time domain. From curves plotted in Figure 10, one can see that control models have the ability to make the vehicle follow the circular path. The lateral deviation of the vehicle is better controlled at about time $t = 6.0$ s. The heading deviation of the vehicle is controlled to the stable value of about 0.7 degree at $t = 11$ s. The longitudinal velocity of the vehicle is also better controlled (see Figure 10(d)).

Figure 11(a) shows time domain variations of steering angles of wheels of the vehicle in the circular path-following motion. As shown in Figure 11(a), control models can continuously execute self-adaptive adjustment of steering angles of four wheels. In the initial stage, all wheels turn in the same positive direction so that the vehicle can travel a shorter distance to the planned path, compared with the standard front wheels steering vehicles. Steering angles of front and rear wheels increase firstly and decrease afterwards in this stage. It is interesting to note that steering angles of rear wheels become zeros at about time $t = 6.0$ s, which accounts for the critical time that the lateral deviation of the vehicle is diminished, as shown in Figure 10(b). In the following five seconds, steering angles of front and rear wheels continuously decrease, and front and rear wheels turn in the opposite directions to fit into the orientation adjustment of the vehicle since the vehicle moves in a circular path with the constant longitudinal velocity of 36 km/h.

As observed in Figure 11(a), the steering angles of front and rear wheels remain constantly in the time intervals about $t = 10$ s to $t = 20$ s and $t = 25$ s to $t = 30$ s, respectively. It should be pointed out that in above time intervals, larger longitudinal velocities of the vehicle may result in larger steering angles of front and rear wheels. The phenomena can be simply understood as follows. In a linear tire model used, the steering angle of the tire is related to the slip angle and the velocity angle. Simulation results indicate that the velocity angles of all tires are invariant after about time $t = 10$ s (see Figure 11(b)). Note that the vehicle undergoes the uniform circular motions in above time intervals. The lateral forces of tires then act as the centripetal forces causing the circular motion of the vehicle. On the other hand, the lateral tire force is assumed to be proportional to the tire slip angle in this research. Accordantly, larger steering angles of wheels are required as the vehicle follows the circular path at higher velocities. In comparison with results plotted in Figures 11(a) and 11(b), it can be found that the velocity

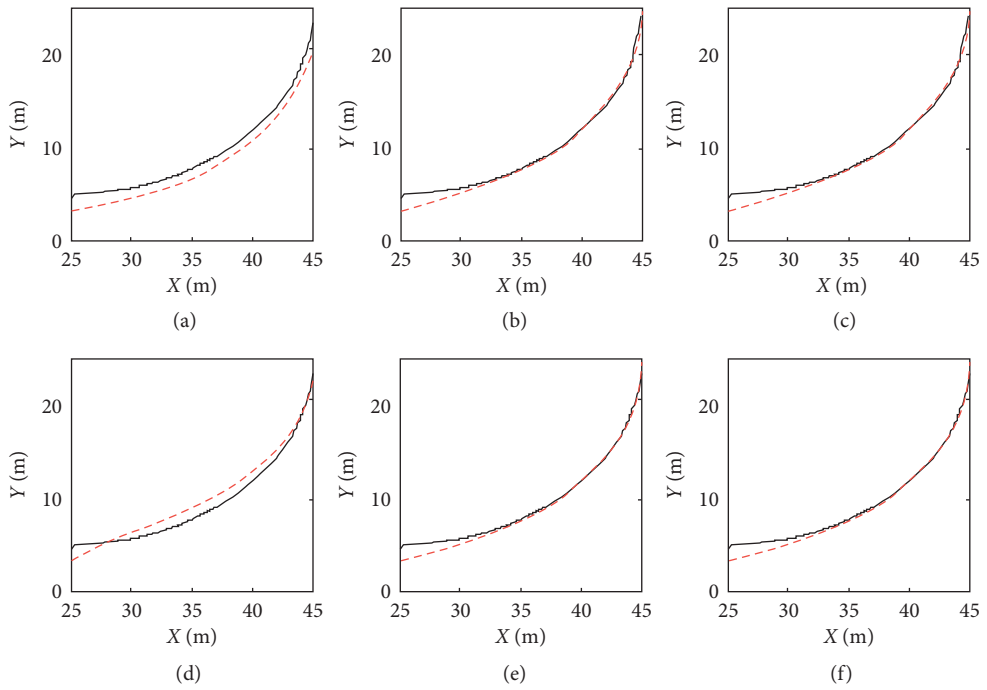

	c_d	k_d	c_θ	k_θ	c_v
(a)	4.0	1.0	2.0	1.0	1.0
(b)	2.0	1.0	2.0	1.0	1.0
(c)	1.4	1.0	2.0	1.0	1.0
(d)	0.5	1.0	2.0	1.0	1.0
(e)	2.0	1.0	1.4	1.0	1.0
(f)	2.0	1.0	0.5	1.0	1.0

Figure 4: The trajectories of coordinates X_C and Y_C govern by equation (12) with a circular reference path and various control parameters introduced.

Table 1: Parameters used in the vehicle model.

Notation	Value	Unit
Vehicle mass m	1080	kg
Inertia moment J	996	kg·m^2
Cornering stiffness of front tire C_α^f	−68245	N/rad
Cornering stiffness of rear tire C_α^r	−70245	N/rad
Half of front track width a	0.79	m
Half of rear track width b	0.84	m
The distance from mass center of the vehicle to front axles l_f	1.35	m
The distance from mass center of the vehicle to rear axles l_r	1.21	m
Air density ρ	1.2258	N/s^2/m^4
Air drag coefficient C_d	0.3	—
Frontal cross-sectional area A	2.5	m^2
Tire rolling resistance C_f	0.01	—
Gravitational constant g	9.8	m/s^2

angle constitutes a large portion of the steering angle of the wheel. In that sense, the steering angles of front wheels are larger than those of rear wheels, as shown in Figure 11. Note that the tire velocity angle is defined as the angle between the velocity direction of the wheel center and the longitudinal direction of the vehicle (see Figure 11(b)).

Results for the vehicle velocity and acceleration in the circular path-following motion are, respectively, shown in Figures 12(a) and 12(b). From Figure 12(a), one can see that the vehicle is in circular motion with uniform velocities in time intervals $t = 5$ s to 20 s and $t = 25$ s to 30 s, respectively. Considering the circular motion condition, the vehicle

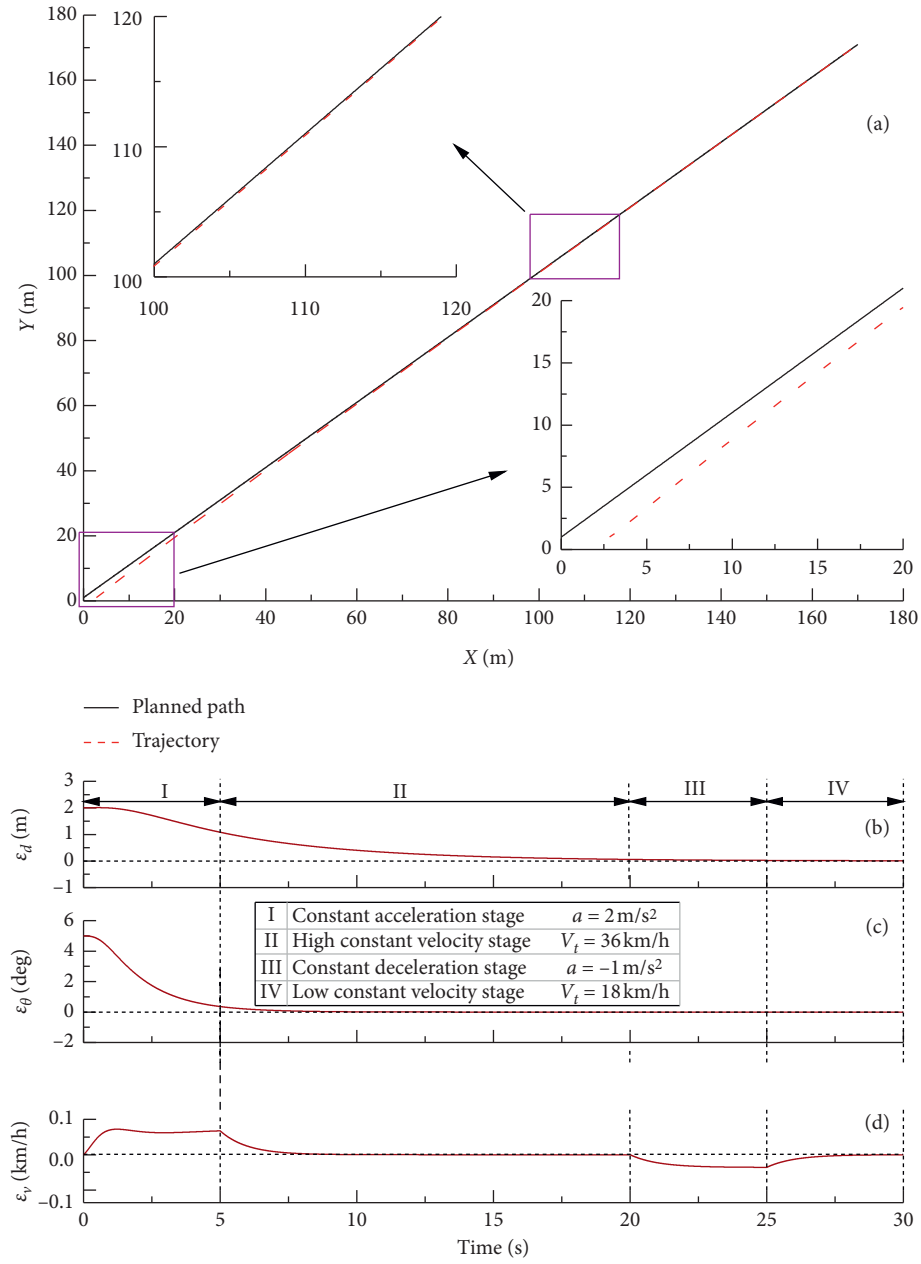

Figure 5: The control performances of the vehicle in the straight path-following motion.

longitudinal velocity is simply calculated by a multiplication of angular velocity ω (the yaw rate of the vehicle) with the path radius $R = 20$ m. It can be observed in Figure 12(d) that the angular velocity ω is about 0.5 rad/s and 0.25 rad/s in two time intervals, respectively. Analytical results for the vehicle velocities are thus, respectively, 10 m/s and 5 m/s, namely, 36 km/h and 18 km/h. Obviously, analytical results are in good agreement with numerical results plotted in Figure 12(a). Similarly, analytical centripetal accelerations, namely, lateral acceleration, can be simply calculated by a multiplication of the square of angular velocity ω with the path radius R. They are 5 m/s^2 and 1.25 m/s^2 in two time intervals, respectively, and approximately identical with their numerical solutions shown in Figure 12(b).

The lateral deviation of the vehicle can be effectively diminished by adjusting the control parameter k_d. It can be seen in Figure 13(a) that the larger k_d is used, and the smaller ε_d is obtained. The control parameter k_d also affects the convergence of the lateral deviation. As shown in Figure 13(a), the convergence can be accelerated by using large k_d, to some extent. By contrast, a fast convergence rate is achieved by small c_d, as shown in Figure 13(b). Similar effects of control parameters k_θ and c_θ are found in Figures 13(c) and 13(d). Figures 13(c) and 13(d), respectively, show the effects of control parameters k_θ and c_θ on the heading deviation of the vehicle in the circular path-following motion. Figure 13(e) shows the effect of the control parameter c_v on the velocity deviation of the vehicle in the circular path-following motion.

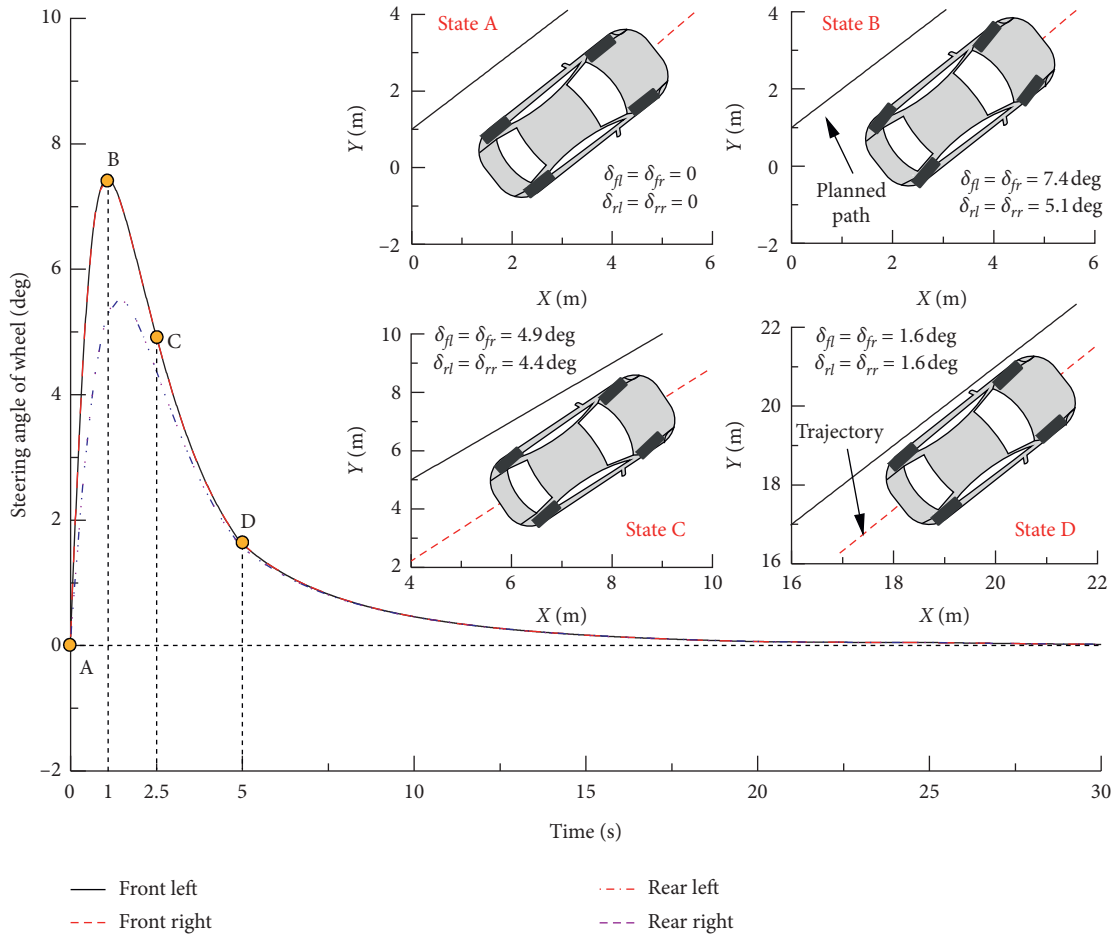

Figure 6: Time histories for steering angles of wheels of the vehicle in the straight path-following motion.

It reveals that there are no obvious differences between the stable velocity deviations of the vehicle corresponding to various parameters c_v

Based on results obtained above, it can be inferred that the wheels of the vehicle turn in a coordinated mode. Control models accommodate various steering modes. Several typical steering modes are shown in Figure 14. The vehicle is assumed to be initially at the state I. To follow the path, it turns in the way that the front steering angles are in the opposite direction to the rear steering angles. However, the wheels turn in the same direction if the vehicle starts from the states II, III, IV, and V. In most situations, the front wheels turn dominantly, while the rear wheels assist the steering action. It is interesting to note here that the rear wheels can also act as the leading wheels in turning; see the curves in dark magenta corresponding to the state IV. Moreover, the vehicle can turn all four wheels equally in the same direction so that it approaches the path as quickly as possible. The analysis reveals that the steering largely depends on the initial states of the vehicle. Figure 15 shows the trajectories of the path-following vehicle under dynamic conditions representing different radii of the circular path and initial deviations of the vehicle from the path. From Figures 14 and 15, it can be concluded that control models have good performances with robustness.

5.3. Case 3: Sinusoidal Path. In the above two cases, the paths have constant curvatures. By contrast, a planned path with continuously variable curvatures is followed by the vehicle in the third case. For this purpose, consider a sinusoidal path

$$Y - a_s \cos\left(\frac{2\pi X}{b_s}\right) - c_s = 0, \tag{26}$$

where constants $a_s = 10$, $b_s = 90$, and $c_s = 10$. The vehicle follows the path from an initial state indicating the lateral deviation $\varepsilon_d = -2$ m, the heading deviation $\varepsilon_\theta = -5$ degree, and the velocity deviation $\varepsilon_v = -2$ m/s. It is assumed that the vehicle starts at the velocity of 8 m/s. Initial conditions for dynamic simulation are −2, 45, −5, 8, 0, and 0. Control parameters are $c_d = 5.0$, $k_d = 1.5$, $c\theta = 1.5$, $k\theta = 21.0$, and $c_v = 0.5$. To fit into the sinusoidal path-following motion, the planned velocity of the vehicle varies with time in the way.

$$V_t = a_t \cos\left(\frac{2\pi X}{b_t}\right) + c_t, \tag{27}$$

where constants a_t, b_t, and c_t are 2.5, 45, and 12.5, respectively. Note that V_t is in m/s.

Dynamic analysis is carried out, and main results are plotted in the following figures. Figure 16(a) shows the trajectory of the vehicle under control. As shown in

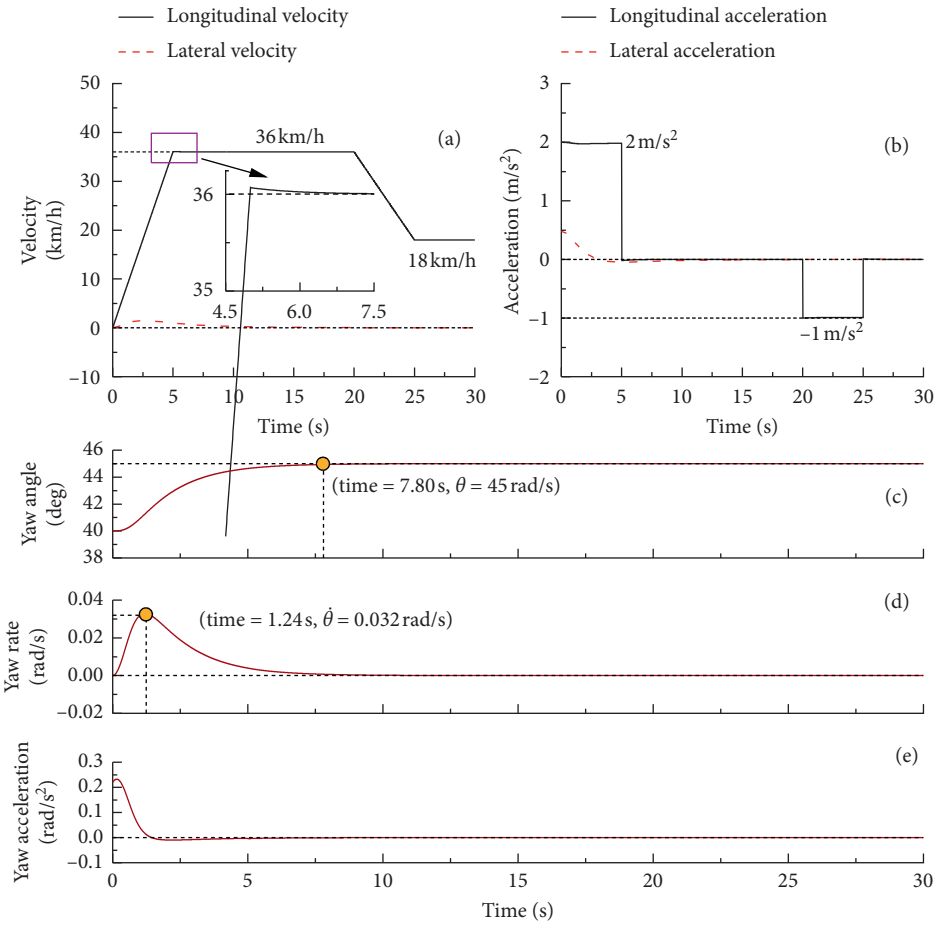

FIGURE 7: Time histories for several state variables of the vehicle in the straight path-following motion: (a) velocity, (b) acceleration, (c) yaw angle, (d) yaw rate, and (e) yaw acceleration.

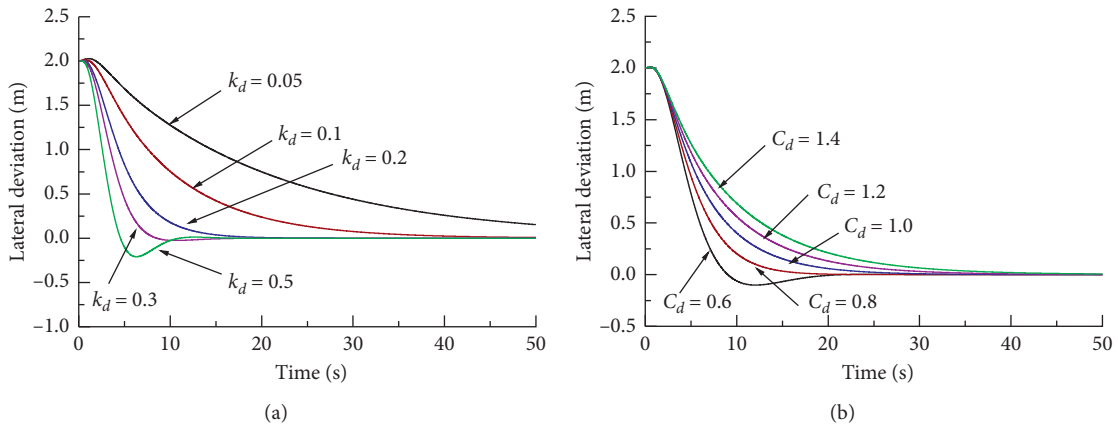

FIGURE 8: Comparisons of convergence rate of the lateral deviation with various control parameters: effects of (a) k_d and (b) c_d.

Figure 16(a), the vehicle moves towards the planned path. After the vehicle is close to point A on the path, it can better follow the path against with curvature variations of the path. The maximum lateral deviation from the path is about 2.0 cm (see Figure 16(d)). Moreover, the vehicle controlled is capable of tracking the velocity profiles within about 0.1 km/h (see Figure 16(f)). As shown in Figure 16(e), the heading deviation fluctuates obviously but falls within an allowable range. Note that the heading deviation has the extreme value near the zero slope points on the path. The reason may be that the vehicle turns sharply and quickly at expense of the heading deviation.

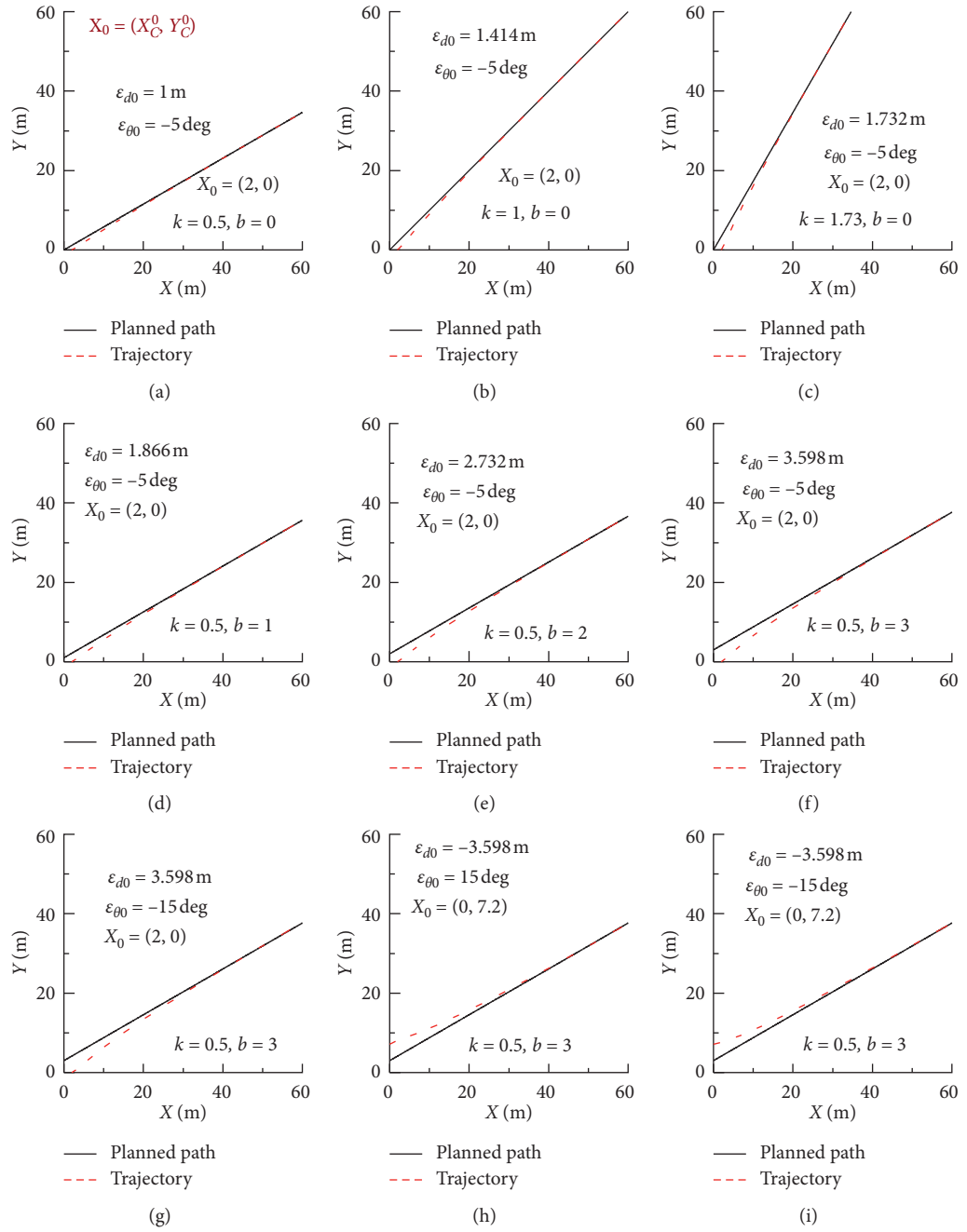

Figure 9: The straight path-following motion of the vehicle under different dynamic conditions.

Figure 17 shows time domain responses of several state variables of the vehicle under path-following control. To accord with the curvature of the path, the lateral velocity of the vehicle approximately varies in a periodic way. It has extreme values of about 0.91 m/s or −0.04 m/s near the zero slope points on the path, as shown in Figure 17(a). Figure 17(b) reveals that the yaw rate of the vehicle comparatively slowly changes with time. In that sense, the yaw motion of the vehicle contributes small towards the velocity angle of the wheel. It is thus reasonable to conclude that the velocity angle of the wheel can be mainly approximated by the velocity angle of the vehicle (see Figure 17(c)).

As stated in Case 2, the velocity angle of the wheel constitutes a large portion of the steering angle of the wheel. It is also true in this case, as shown in the curves plotted in Figures 17(c) and 17(d). Figure 17(d) shows time histories for the steering angles of four wheels of the vehicle under the path-following control. From Figure 17(d), one can see that

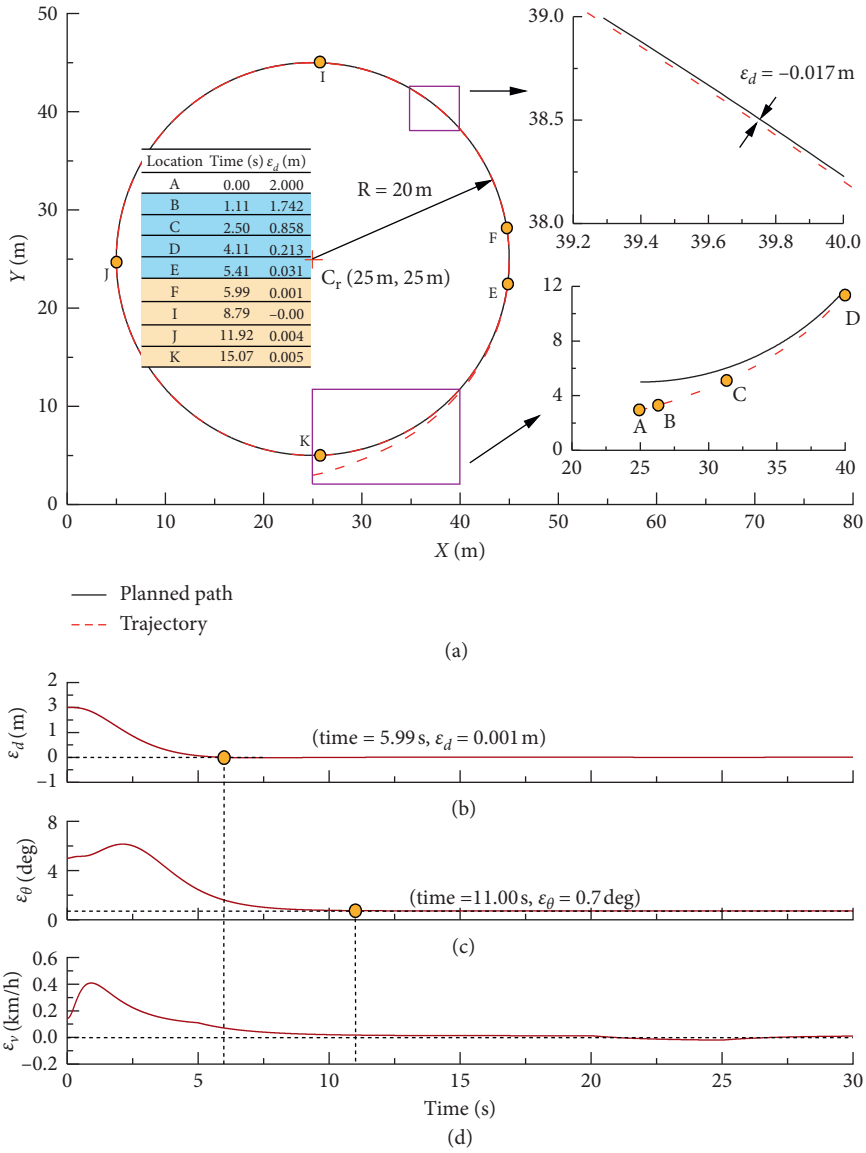

Figure 10: The control performances of the vehicle in the circular path-following motion.

the steering angles of the wheels at points B, D, F, and H are approximately equal and all close to zeros. The reasons are given as follows. The curvatures of the path at these points are zeros (see Figure 16(c)). In that sense, the vehicle approximately follows a straight path near these points. According to results obtained in Case 1, the steering angles of four wheels are all equal to zeros as the vehicle travels the straight path in a stable state. However, owing to the curvature variation of the path and the heading deviation, the steering angles of four wheels are nearly zeros (not absolute zeros). In addition, the front wheels have larger steering angles at points *C* and *G* compared with points *A* and *E*. They are caused by larger lateral velocities of the vehicle passing through points *C* and *G*.

6. Dynamic Results with a Fine Vehicle Model in CarSim

Control models are tested and examined in a complex situation with a fine vehicle model established in CarSim and a complex planned path. For modeling, the vehicle has sprung mass of 1040 kg, roll inertia of 606.1 kg·m^2, pitch inertia of 1523 kg·m^2, and yaw inertia of 1523 kg·m^2. Other parameters of the vehicle are listed in Table 2. The planned path is shown in Figure 18. It is composed of straight and curved segments, as well as a sinusoidal segment. The velocity of the vehicle in the path-following motion varies in a stepwise way in m/s as

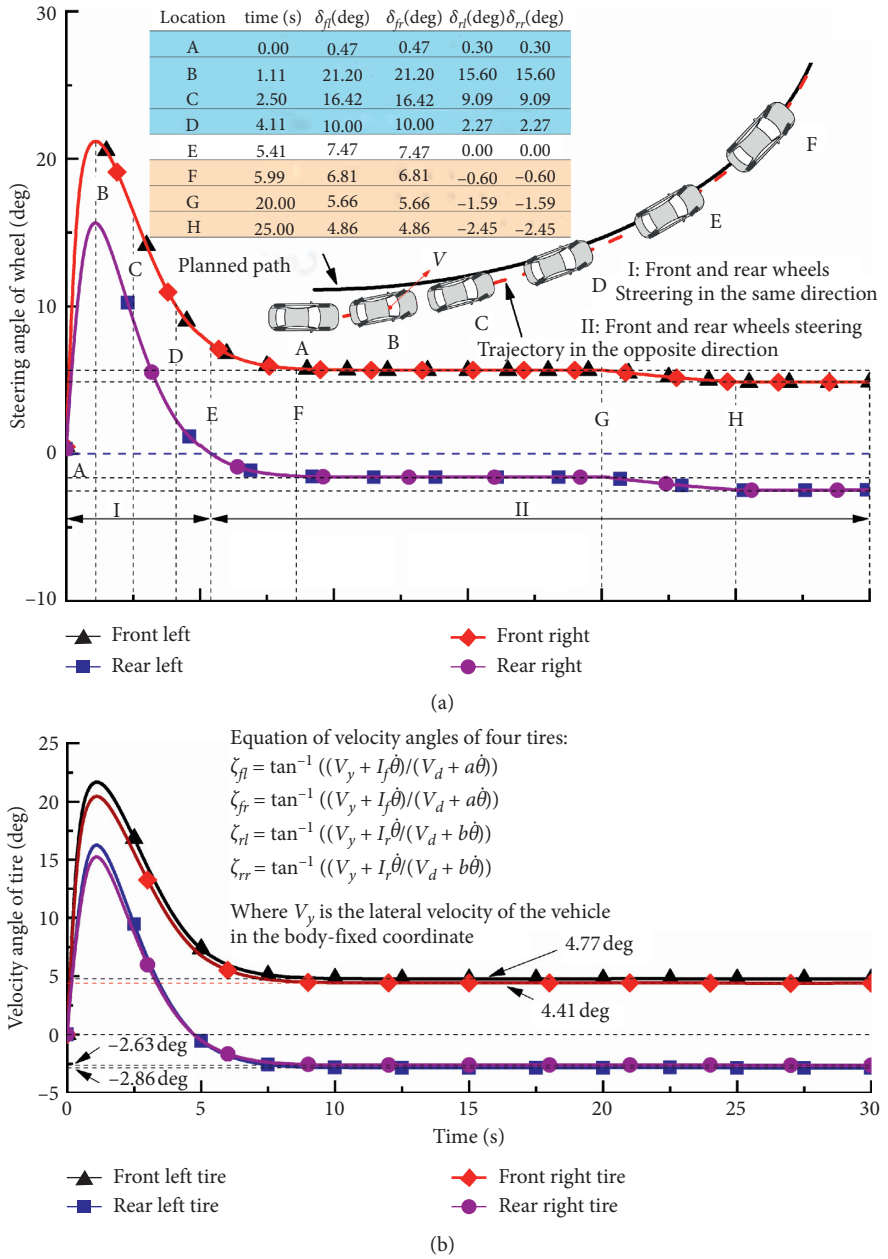

Figure 11: Time histories for wheel steering angles and velocity angles of the vehicle in the circular path-following motion.

$$V_t(t) = \begin{cases} 2t, & t < T_1, \\ 10, & T_1 \le t < T_2, \\ 0.5t - 6, & T_2 \le t < T_3, \\ 15, & T_3 \le t < T_4, \\ -0.9t + 57.3, & T_4 \le t < T_5, \\ 6, & T_5 \le t, \end{cases} \tag{28}$$

where constants T_1, T_2, T_3, T_4, and T_5 are 5.0 s, 32.0 s, 42.0 s, 47.0 s, and 57.0, respectively. The vehicle initially deviates from the path by $\varepsilon_d = 1.0$ m. Thus, initial simulation conditions of $X_{C0} = 0$, $Y_{C0} = 1.0$, $\theta_0 = 0$, $\dot{X}_{C0} = 0$, $\dot{Y}_{C0} = 0$, and $\dot{\theta}_0 = 0$ are taken. Control parameters $c_d = 18$, $k_d = 5$, and $c_v = 1.5$ are used in the vehicle path-following analysis. To fit into the vehicle path-following in sinusoidal segment, control parameters $c_\theta = 4$ and $k_\theta = 20$ are used while they are 12 and 5 in the straight or circular segment of the path,

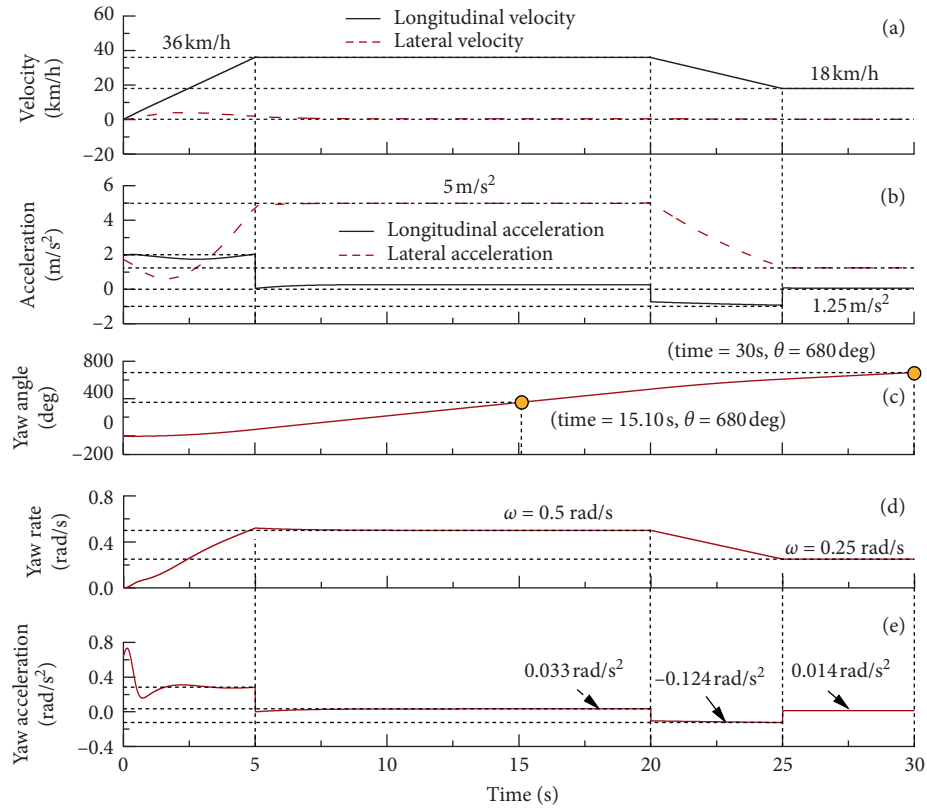

FIGURE 12: Time histories for several state variables of the vehicle in the circular path-following motion: (a) velocity, (b) acceleration, (c) yaw angle, (d) yaw rate, and (e) yaw acceleration.

respectively. Simulations are performed by using above parameters and variable conditions. Main results are obtained and analyzed below.

Figure 19 shows variations of the vehicle state against with the planned path in the time domain. As observed in Figure 19(a), the vehicle controlled approaches the path at a short starting period. After that, the vehicle runs along the path with the maximum lateral deviation of no more than 0.1 m and the maximum heading deviation of nearly 10 degree (see Figure 19(b)). In this process, the vehicle velocities deviate from the desired ones within an allowable range [−0.5 0.5], whether the vehicle runs at low or high speeds (see Figure 19(c)). Moreover, the heading deviation of the vehicle obviously changes at some locations, e.g., junction points from straight to curved segments of the path. It may be caused by discontinuous curvatures of the path at these points. The variations of the path curvature against with the travelling distance S of the vehicle are illustrated in Figure 20(b). Figure 20 shows the trajectory of the path-following vehicle against with curvature variations of the path. It is concluded that control models still take effects in this complex problem.

Figure 21 shows time histories for steering angles and longitudinal forces of wheels of the vehicle in the path-following control. In control, front and rear wheels steer and cooperate with each other in dynamic conditions. As observed in Figure 21(a), all wheels steer towards the same direction when the vehicle largely deviates from the path in the starting period. In this way, the vehicle quickly approaches the path without large heading deviations. By contrast, the rear wheels steer in the opposite direction to the front wheels when the vehicle stably runs along circular segments of the path. Meanwhile, an interesting phenomenon can be found in Figure 21(a) that the steering angle of the front wheel is somewhat larger than that of the rear wheel. Possible reasons are similar with the ones provided in Section 5.2.

Results for the velocities and accelerations of the vehicle that follows the compound path are shown in Figures 22 and 23, respectively. It can be seen in Figure 22(a) that the vehicle always runs along the path with time-varying variables as expected. Importantly note that the vehicle stably follows the circular path with radius $R = 15$ m at a constant velocity of $V_x = 6$ m/s after simulation time $t = 57$ s. In the circular motion law, the analytical yaw rate can be calculated by using V_x and R. Dividing V_x by R leads to the yaw rate of 0.4 rad/s of the vehicle, namely, about 23 deg/s. The analytical result for the yaw rate of the vehicle is in good agreement with simulation results plotted in Figure 22(c). Similarly, the lateral acceleration of the vehicle can be analytically calculated and the same as the one obtained numerically, as shown in Figure 23. Control models capture main dynamic behaviors of the vehicle in this path-following control. Control models are validated in the complex situation.

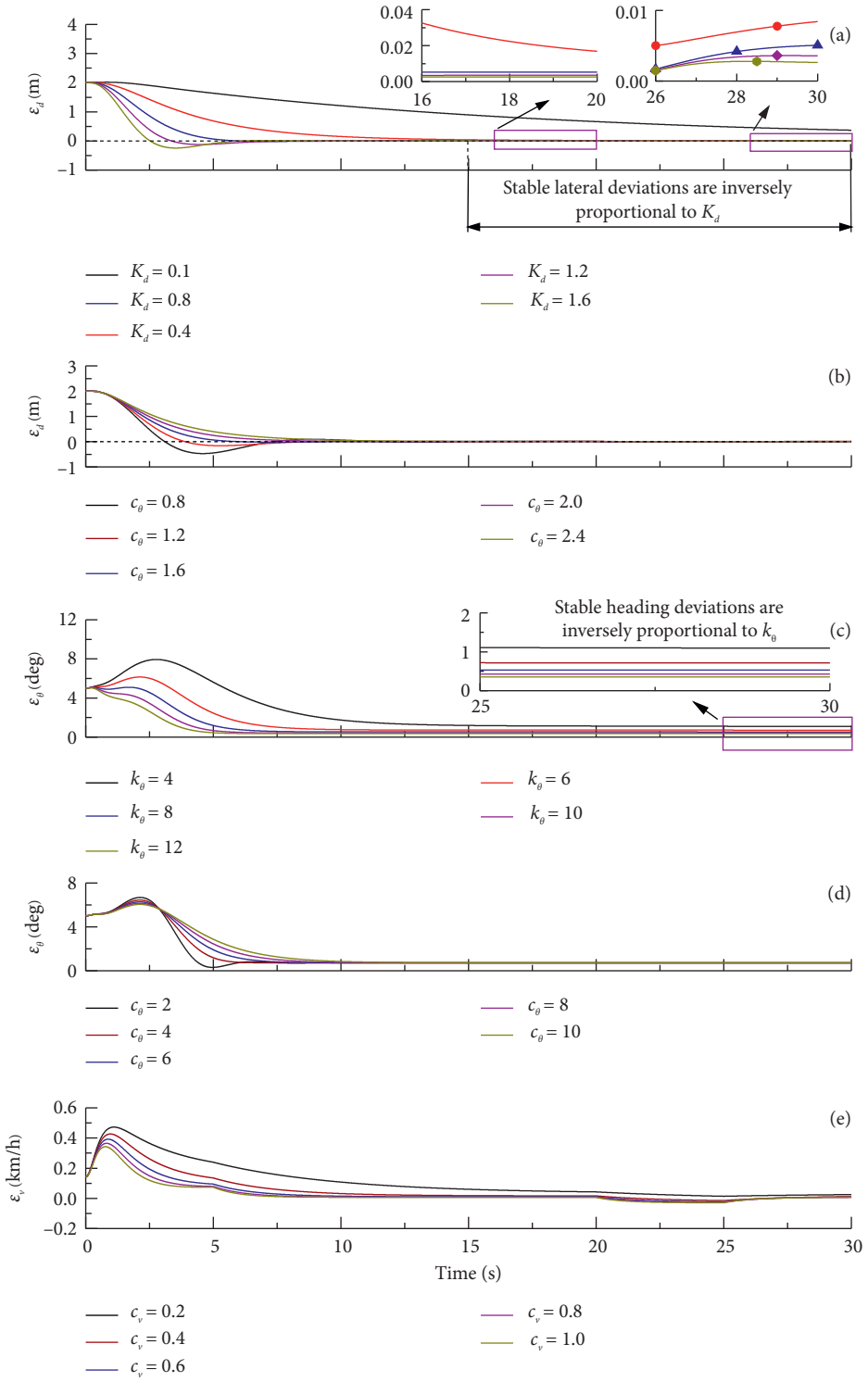

FIGURE 13: Effects of control parameters on three deviations of the vehicle in a circular path-following motion: (a) parameter k_d, (b) parameter c_d, (c) parameter k_θ, (d) parameter c_θ, and (e) parameter c_v.

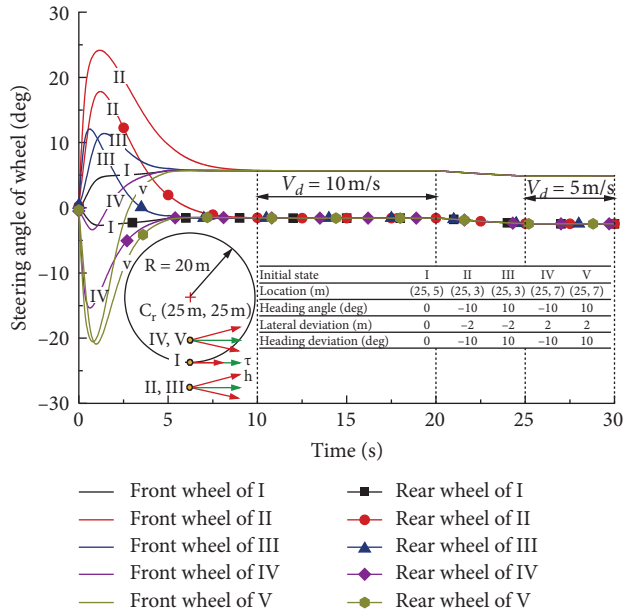

Figure 14: Time histories for steering angles of the vehicle that follows the circular path from different initial states.

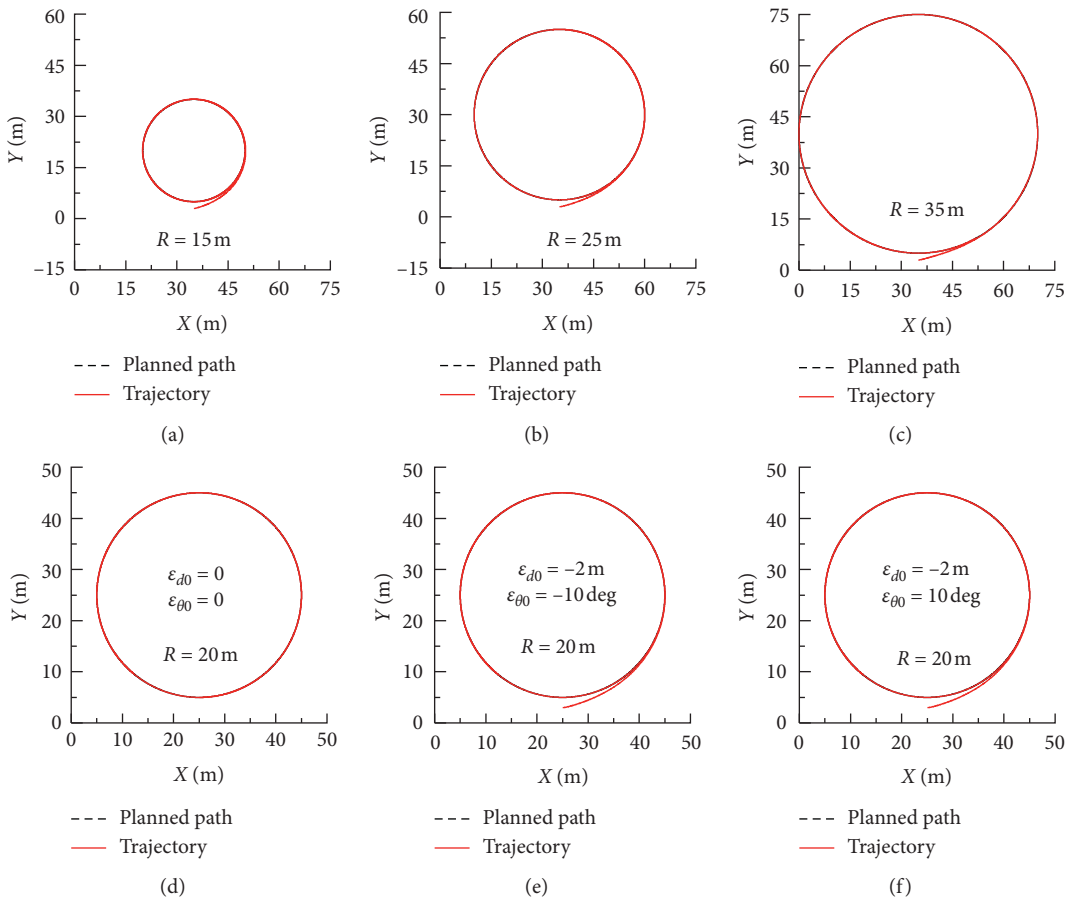

Figure 15: Continued.

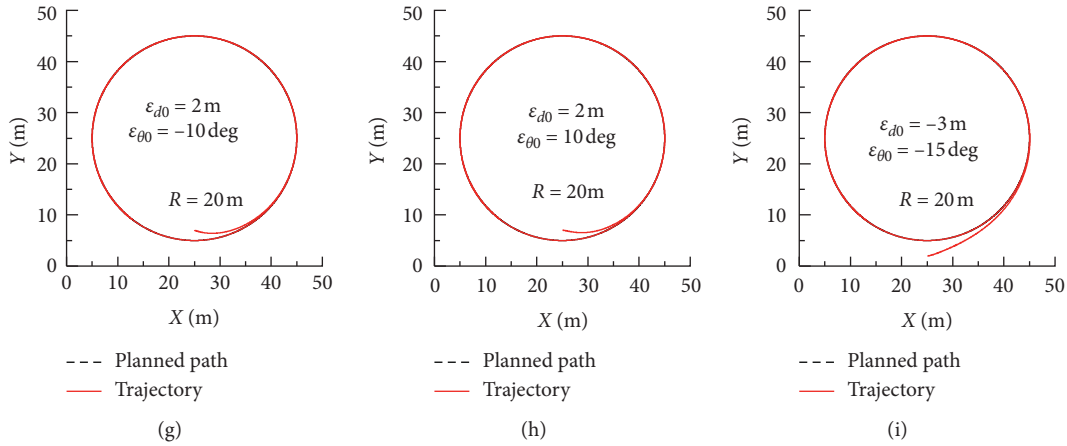

Figure 15: The circular path-following motions of the vehicle under different dynamic conditions.

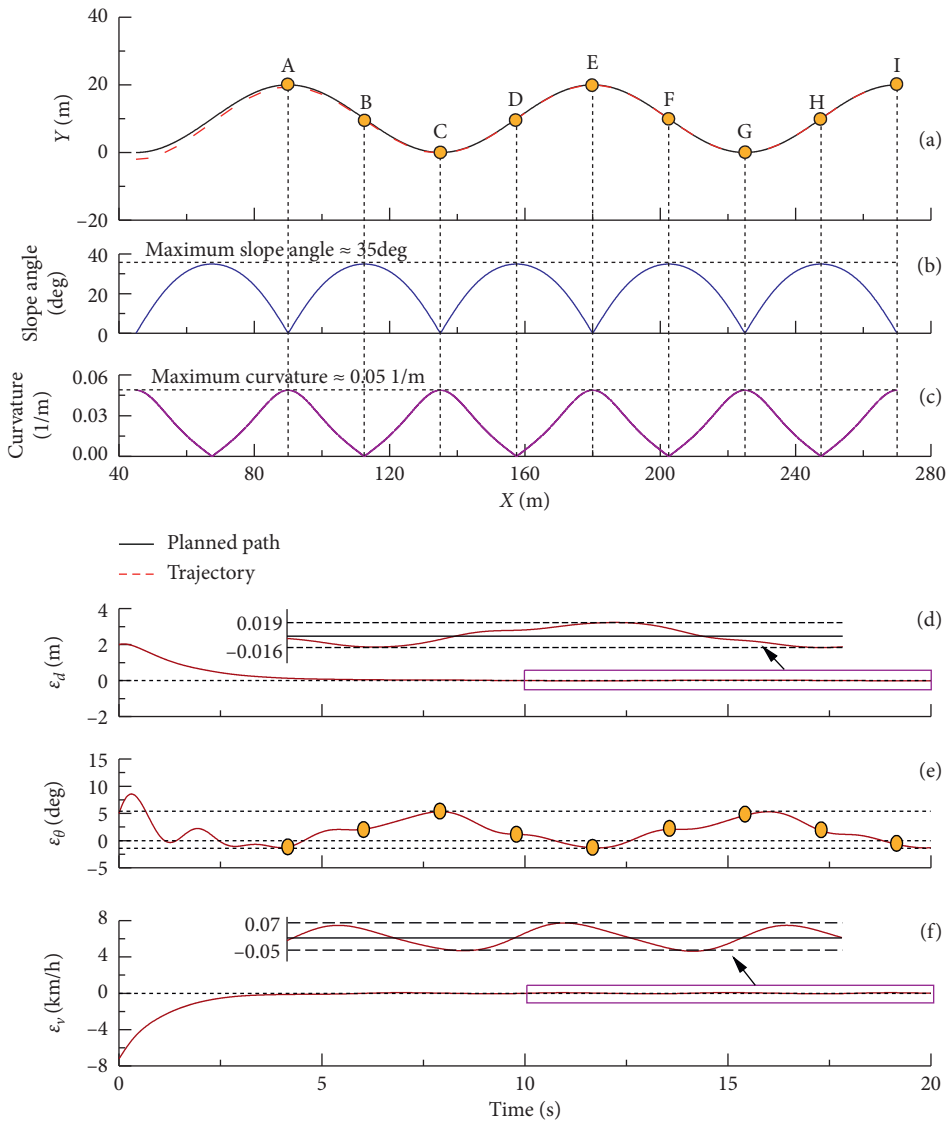

Figure 16: The control performances of the vehicle in the sinusoidal path-following motion.

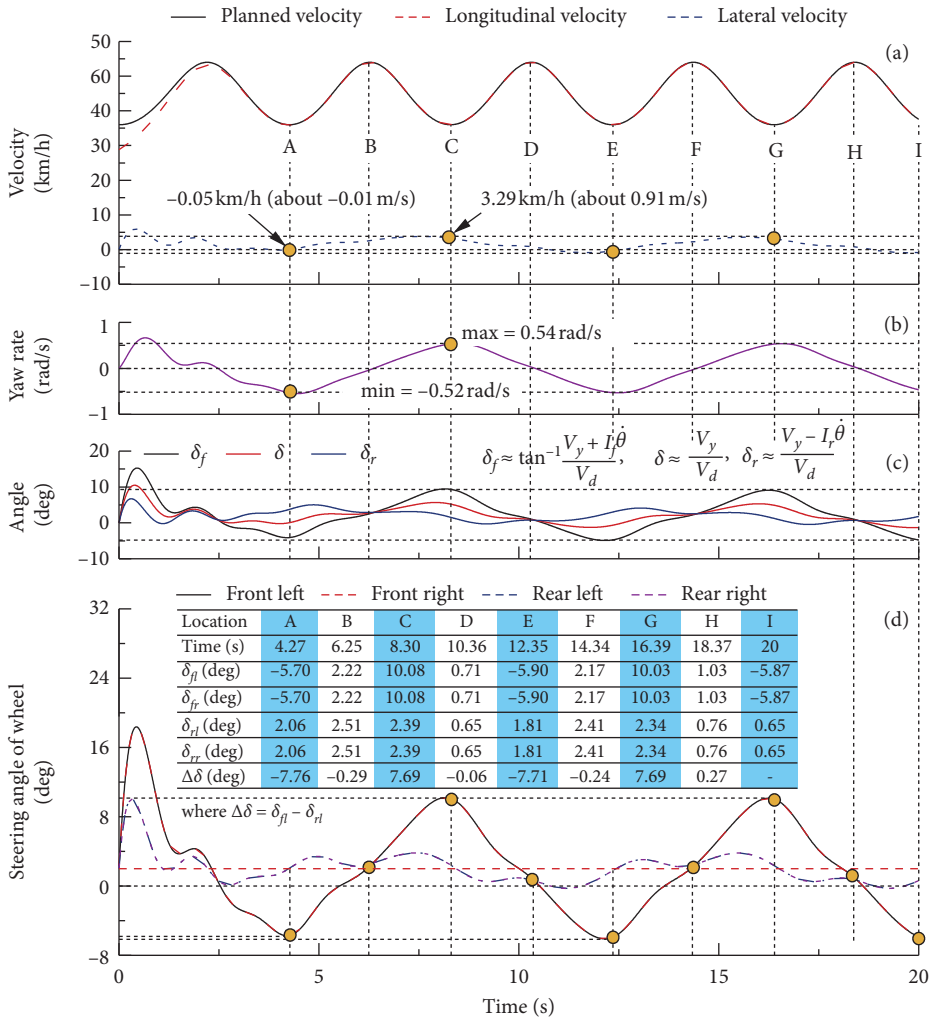

Location	A	B	C	D	E	F	G	H	I
Time (s)	4.27	6.25	8.30	10.36	12.35	14.34	16.39	18.37	20
δ_{fl} (deg)	−5.70	2.22	10.08	0.71	−5.90	2.17	10.03	1.03	−5.87
δ_{fr} (deg)	−5.70	2.22	10.08	0.71	−5.90	2.17	10.03	1.03	−5.87
δ_{rl} (deg)	2.06	2.51	2.39	0.65	1.81	2.41	2.34	0.76	0.65
δ_{rr} (deg)	2.06	2.51	2.39	0.65	1.81	2.41	2.34	0.76	0.65
$\Delta\delta$ (deg)	−7.76	−0.29	7.69	−0.06	−7.71	−0.24	7.69	0.27	-

Figure 17: Time histories for several variables of the vehicle in sinusoidal path-following motion.

Table 2: Main parameters for the vehicle model established in CarSim.

Notation	Value	Unit
Unsprung mass(both sides)	60	Kg
Half of front track width	0.77	M
Half of rear track width	0.77	M
Distance from mass center of the vehicle to front axle	1.1	M
Distance from mass center of the vehicle to rear axle	1.24	M
Mass center of unladen sprung mass	350	M
Tires type	175/65 R14	—
Effective rolling radius of tire	0.284	m
Unloaded radius of tire	0.292	m
Air density	1.2258	$N/s^2/m^4$
Air drag coefficient	0.3	—
Frontal cross-sectional area	2.5	m^2
Tire rolling resistance	0.01	—
Gravitational constant	9.8	m/s^2
Friction coefficient	0.85	—

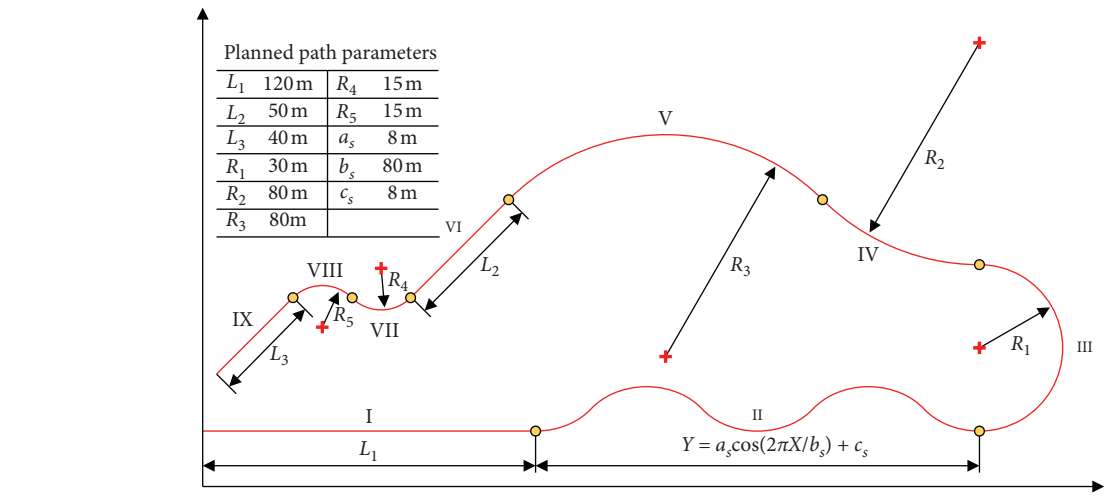

Figure 18: Schematic of a complex path.

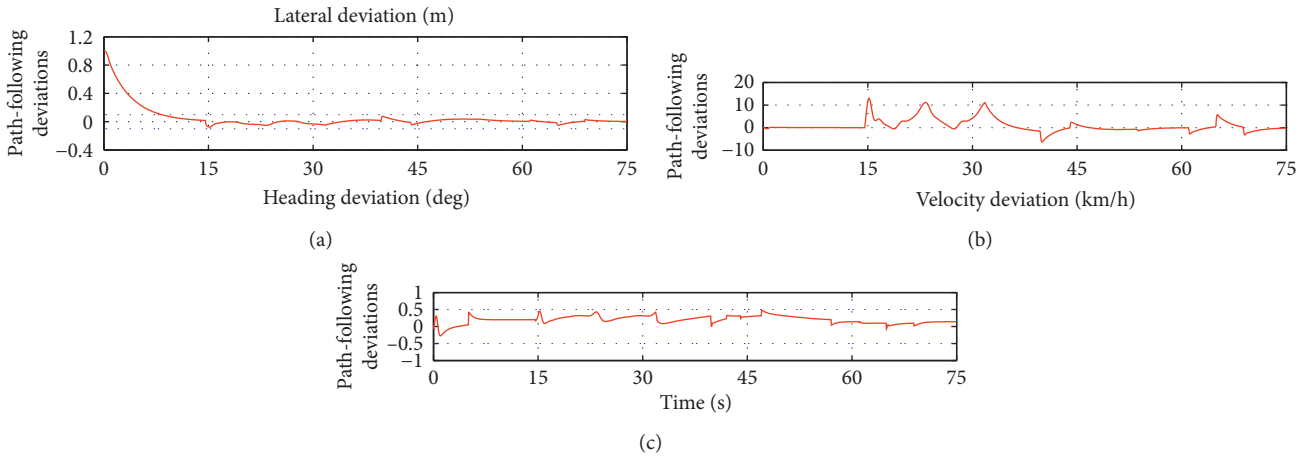

Figure 19: Time histories for three deviations of the vehicle under the path-following control.

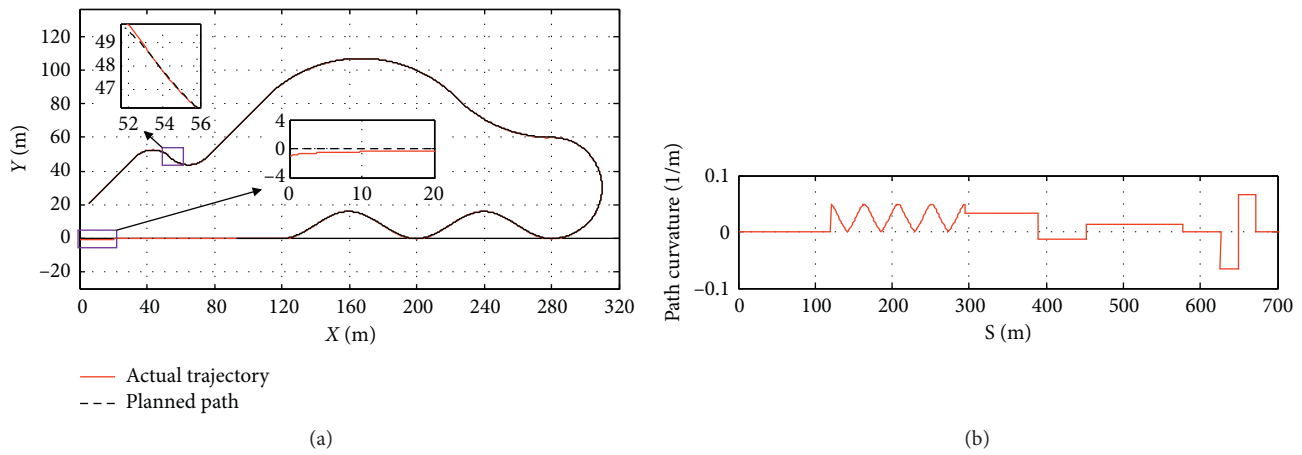

Figure 20: The trajectory of the path-following vehicle against with curvature variations of the path.

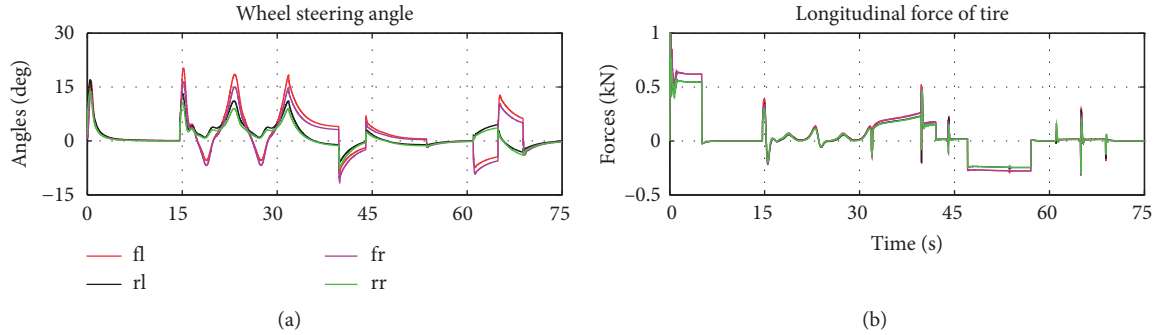

Figure 21: Time histories for steering angles and longitudinal forces of the wheels of the vehicle in the path-following control.

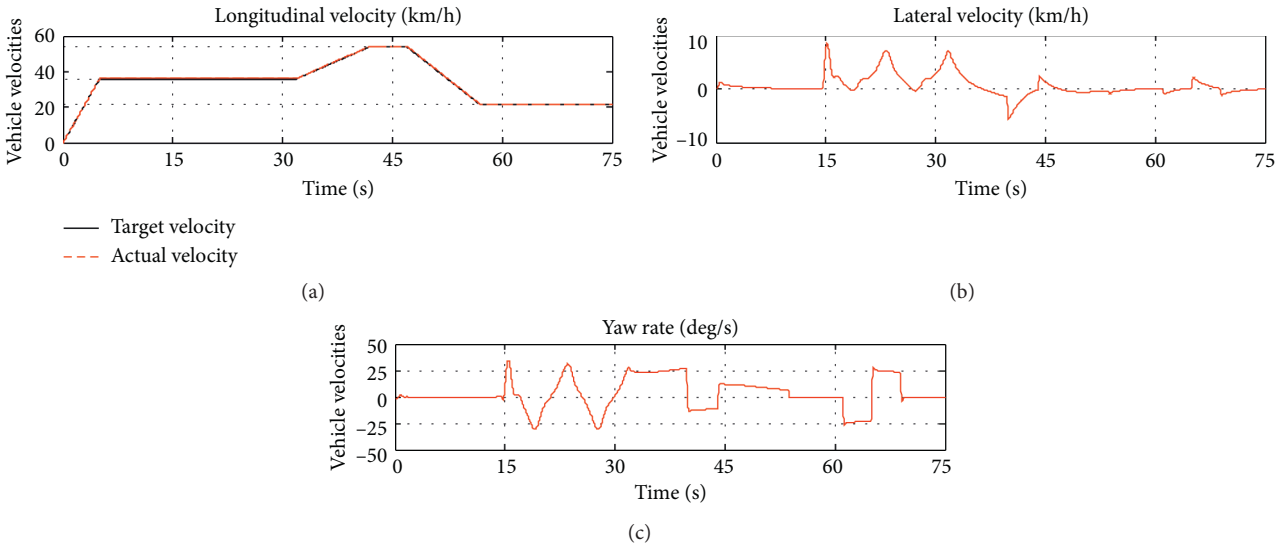

Figure 22: Time histories for longitudinal and lateral velocities and yaw rate of the path-following vehicle.

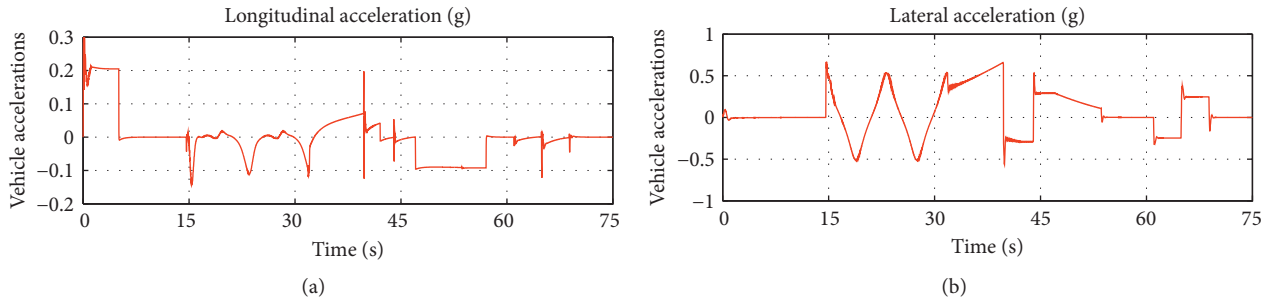

Figure 23: Time histories for longitudinal and lateral accelerations of the path-following vehicle.

7. Conclusions

Control models are understood and examined in various aspects. Control models can take effects and maintain a good control level against with different planned paths, including the straight, circular, and sinusoidal paths, as well as a compound path. Control models provide multiple turning modes, which depend on initial states of the vehicle.

Control performances of the path-following vehicle are shown with numerical studies. In the straight and circular path-following motions, numerical results are in good agreement with those obtained analytically. As following

complex paths with continuous variable or stepwise constant curvatures, the vehicle can be better controlled. Numerical results reveal that control models incorporate coupled effects of the path-following vehicle in longitudinal, lateral, and rotational directions.

Control parameters have strong influence on the path-following performance. Constant k_d allows an active control of the vehicle lateral deviation. The lateral deviation of the vehicle can be diminished by adjusting constant k_d. The convergence rate of lateral deviation depends on constants both k_d and c_d. Control parameters k_θ, c_θ, and c_v have similar effects on the heading and velocity deviations.

However, there leaves some meaningful jobs needed to be done next. For example, the effects of motor properties should be included in the current control model since drive torque in motors can directly affect longitudinal dynamics of the vehicle. In addition, in order to achieve better tire force allocation, the interaction between the longitudinal tire force and lateral tire force will be considered in the path-following control model. Experiments that test control models are also carried out as soon as possible. All jobs mentioned above will be reported as a series of individual papers in the future.

Appendix

A. Explicit Expressions in Relevant Equations

In this appendix, some important expressions are explicitly given. In equation (4), there are

$$\begin{aligned} f_x &= F_l^f \cos\delta_f - F_s^f \sin\delta_f + F_l^r \cos\delta_r - F_s^r \sin\delta_r - F_w - F_f, \\ f_y &= F_l^f \sin\delta_f + F_s^f \cos\delta_f + F_l^r \sin\delta_r + F_s^r \cos\delta_r, \\ M_z &= \left(F_l^f \sin\delta_f + F_s^f \cos\delta_f\right)a + \left(F_l^r \sin\delta_r + F_s^r \cos\delta_r\right)b, \end{aligned} \tag{A.1}$$

where a and b denote half of the front and rear track widths. F_s^f and F_s^r are lateral forces of front and rear wheels and can be determined in a simple way as [6, 22]

$$F_s = C_\alpha \alpha, \tag{A.2}$$

where C_α is the tire cornering stiffness and α is the tire slip angle, and F_w and F_f are aerodynamic and rolling resistances, which can be calculated as [4, 18, 23]

$$\begin{aligned} F_w &= C_d A \rho V_d^2, \\ F_f &= C_f m g, \end{aligned} \tag{A.3}$$

in which ρ is the air density, C_d is the drag coefficient, A is the frontal cross-sectional area of the vehicle, V_d is the longitudinal velocity of the vehicle, C_f is the rolling drag coefficient, and g is the gravitational acceleration constant.

In equation (12), $\overline{M}$ and $\overline{F}$ are, respectively, defined as follows:

$$\overline{M} = \begin{bmatrix} \frac{\partial f_v}{\partial \dot{X}_C} & \frac{\partial f_v}{\partial \dot{Y}_C} & 0 \\ \frac{\partial f_d}{\partial X_C} & \frac{\partial f_d}{\partial Y_C} & \frac{\partial f_d}{\partial \theta} \\ \frac{\partial f_\theta}{\partial X_C} & \frac{\partial f_\theta}{\partial Y_C} & \frac{\partial f_\theta}{\partial \theta} \end{bmatrix}, \tag{A.4}$$

$$\overline{F} = -\begin{bmatrix} \frac{\partial f_v}{\partial \theta}\dot{\theta} + c_v \varepsilon_v + \dot{V}_t \\ \dot{X}^T \mathbf{H}_d \dot{X} + c_d \dot{\varepsilon}_d + k_d \varepsilon_d \\ \dot{X}^T \mathbf{H}_\theta \dot{X} + c_\theta \dot{\varepsilon}_\theta + k_\theta \varepsilon_\theta \end{bmatrix},$$

in which $\mathbf{H}_d$ and $\mathbf{H}_\theta$ are given by

$$\mathbf{H}_d = \begin{bmatrix} \frac{\partial^2 f_d}{\partial X_C^2} & \frac{\partial^2 f_d}{\partial Y_C \partial X_C} & \frac{\partial^2 f_d}{\partial \theta \partial X_C} \\ \frac{\partial^2 f_d}{\partial X_C \partial Y_C} & \frac{\partial^2 f_d}{\partial Y_C^2} & \frac{\partial^2 f_d}{\partial \theta \partial Y_C} \\ \frac{\partial^2 f_d}{\partial X_C \partial \theta} & \frac{\partial^2 f_d}{\partial Y_C \partial \theta} & \frac{\partial^2 f_d}{\partial \theta^2} \end{bmatrix}, \tag{A.5}$$

$$\mathbf{H}_\theta = \begin{bmatrix} \frac{\partial^2 f_\theta}{\partial X_C^2} & \frac{\partial^2 f_\theta}{\partial Y_C \partial X_C} & \frac{\partial^2 f_\theta}{\partial \theta \partial X_C} \\ \frac{\partial^2 f_\theta}{\partial X_C \partial Y_C} & \frac{\partial^2 f_\theta}{\partial Y_C^2} & \frac{\partial^2 f_\theta}{\partial \theta \partial Y_C} \\ \frac{\partial^2 f_\theta}{\partial X_C \partial \theta} & \frac{\partial^2 f_\theta}{\partial Y_C \partial \theta} & \frac{\partial^2 f_\theta}{\partial \theta^2} \end{bmatrix}.$$

In equation (16), $\mathbf{A}$ and $\mathbf{b}$ are, respectively, defined by

$$\mathbf{A} = \begin{bmatrix} \begin{pmatrix} k_l \cos\theta\cos\delta_f - k_l \sin\theta\sin\delta_f \\ +\cos\theta\cos\delta_r - \sin\theta\sin\delta_r \end{pmatrix} & \begin{pmatrix} \cos\theta\sin\delta_f \\ +\sin\theta\cos\delta_f \end{pmatrix} C_\alpha^f & \begin{pmatrix} \cos\theta\sin\delta_r \\ +\sin\theta\cos\delta_r \end{pmatrix} C_\alpha^r \\ \begin{pmatrix} k_l \sin\theta\cos\delta_f + k_l \cos\theta\sin\delta_f \\ +\sin\theta\cos\delta_r + \cos\theta\sin\delta_r \end{pmatrix} & \begin{pmatrix} \sin\theta\sin\delta_f \\ -\cos\theta\cos\delta_f \end{pmatrix} C_\alpha^f & \begin{pmatrix} \sin\theta\sin\delta_r \\ -\cos\theta\cos\delta_r \end{pmatrix} C_\alpha^r \\ \sin\delta_f l_f k_l - \sin\delta_r l_r & -l_f C_\alpha^f \cos\delta_f & l_r C_\alpha^r \cos\delta_r \end{bmatrix},$$

$$\mathbf{b} = \mathbf{M}\overline{M}^{-1}\overline{F} + \begin{bmatrix} \begin{pmatrix} \cos\theta\sin\delta_f + \\ \sin\theta\cos\delta_f \end{pmatrix} C_\alpha^f \zeta_f + \begin{pmatrix} \cos\theta\sin\delta_r + \\ \sin\theta\cos\delta_r \end{pmatrix} C_\alpha^r \zeta_r + \cos\theta\left(F_w + F_f\right) \\ \begin{pmatrix} \sin\theta\sin\delta_f - \\ \cos\theta\cos\delta_f \end{pmatrix} C_\alpha^f \zeta_f + \begin{pmatrix} \sin\theta\sin\delta_r - \\ \cos\theta\cos\delta_r \end{pmatrix} C_\alpha^r \zeta_r + \sin\theta\left(F_w + F_f\right) \\ -l_f C_\alpha^f \zeta_f \cos\delta_f + l_r C_\alpha^r \zeta_r \cos\delta_r \end{bmatrix}, \tag{A.6}$$

where ζ_f and ζ_r are the velocity angles of front and rear tires and l_f and l_r are the distances from the mass center of the vehicle to the front and rear axles.

Data Availability

The figure and table data of simulation results used to support the findings of this study are included within the article.

Conflicts of Interest

The authors declare that they have no conflicts of interest.

Acknowledgments

The authors would like to thank supports from the National Natural Science Foundation of China (no. 51775448), the Project for Innovation Talents of Science and Technology of Sichuan Province (no. 2020JDRC0008), Key Research Project of Sichuan Science and Technology Program (no. 2020YFG0023), the Applied Basic Research Programs of Sichuan Province (no. 2018JY0557), Chengdu Technological Innovation R and D Project (no. 2018-YF05-00813-SN), the Project of State Key Laboratory of Traction Power for Southwest Jiaotong University (no. 2016TPL_Z01), the Open Research Subject of Key Laboratory for Xihua University (no. SZJJ2015-049), and the Fundamental Research Funds for the Central Universities (no. 2682018CX70).

References

[1] Z. Zhang, X. Zhang, H. Pan et al., "A novel steering system for a space-saving 4WS4WD electric vehicle: design, modeling, and road tests," *IEEE Transactions on Intelligent Transportation Systems*, vol. 18, no. 1, pp. 114–127, 2017.

[2] Y. Zhao, F. Feng, and R. Zhang, "Development of a four wheel independent drive and four wheel independent steer electric vehicle," in *Proceedings of the 2015 Sixth International Conference on Intelligent Systems Design and Engineering Applications (ISDEA)*, pp. 319–322, IEEE, Guiyang, China, August 2015.

[3] Y. Liang, Y. Li, Y. Yu, and L. Zheng, "Integrated lateral control for 4WID/4WIS vehicle in high-speed condition considering the magnitude of steering," *Vehicle System Dynamics*, vol. 58, no. 11, pp. 1711–1735, 2020.

[4] C. Hu, R. Wang, Z. Wang, M. Chadli, and F. Yan, "Integrated optimal dynamics control of 4WS4WD electric ground vehicles with tire-road frictional coefficient estimation," in *Proceedings of the 2015 American Control Conference (ACC)*, pp. 5426–5431, IEEE, Chicago, IL, USA, July 2015.

[5] L. Jin, L. Gao, Y. Jiang, M. Chen, Yi Zheng, and K. Li, "Research on the control and coordination of four-wheel independent driving/steering electric vehicle," *Advances in Mechanical Engineering*, vol. 9, no. 4, 2017.

[6] L. Xiong, Z. Yu, Y. Wang, C. Yang, and Y. Meng, "Vehicle dynamics control of four in-wheel motor drive electric vehicle using gain scheduling based on tyre cornering stiffness estimation," *Vehicle System Dynamics*, vol. 50, no. 6, pp. 831–846, 2012.

[7] X. Li, N. Xu, K. Guo, and Y. Huang, "An adaptive SMC controller for EVs with four IWMs handling and stability enhancement based on a stability index," *Vehicle System Dynamics*, pp. 1–24, 2020.

[8] R. Potluri and A. K. Singh, "Path-tracking control of an autonomous 4WS4WD electric vehicle using its natural feedback loops," *IEEE Transactions on Control Systems Technology*, vol. 23, no. 5, pp. 2053–2062, 2015.

[9] R. Oftadeh, M. M. Aref, R. Ghabcheloo, and J. Mattila, "Bounded-velocity motion control of four wheel steered mobile robots," in *Proceeding of the 2013 IEEE/ASME International Conference on Advanced Intelligent Mechatronics*, pp. 255–260, IEEE, July 2013.

[10] M. Udengaard and K. Iagnemma, "Kinematic analysis and control of an omnidirectional mobile robot in rough terrain," in *Proceedings of the 2007 IEEE/RSJ International Conference on Intelligent Robots and Systems*, pp. 795–800, San Diego, CA, USA, October 2007.

[11] P. Dai and J. Katupitiya, "Force control of a 4WS4WD vehicle for path tracking," in *Proceedings of the 2015 IEEE International Conference on Advanced Intelligent Mechatronics (AIM)*, pp. 238–243, IEEE, Busan, South Korea, July 2015.

[12] L. Zhai and S. Dong, "Electronic differential speed steering control for four in-wheel motors independent drive vehicle," in *Proceedings of the 2011 9th World Congress on Intelligent Control and Automation*, pp. 780–783, IEEE, Taipei, Taiwan, June 2011.

[13] W. Xiao, J. Zou, H. Li, and K. Xu, "Smooth trajectory tracking using longitudinal distance constraint for A 4WS4WD unmanned ground vehicle∗," in *Proceedings of the 2019 IEEE International Conference on Robotics and Biomimetics (ROBIO)*, pp. 2105–2110, IEEE, Dali, China, December 2019.

[14] C. Bian, G. Yin, N. Zhang, and L. Xu, "Takagi-sugeno fuzzy model predictive controller design for combining lane keeping and speed tracking of four wheels steering and four wheels drive electric vehicle," in *Proceedings of the 2017 29th Chinese Control and Decision Conference (CCDC)*, pp. 4067–4072, Chongqing, China, May 2017.

[15] S.-T. Peng, "On one approach to constraining the combined wheel slip in the autonomous control of a 4WS4WD vehicle," *IEEE Transactions on Control Systems Technology*, vol. 15, no. 1, pp. 168–175, 2007.

[16] Q. Tan, L. Dong, and H. Yan, "MPC based optimal path-tracking control strategy for 4WS4WD vehicles," in *Proceedings of the IECON 2017-43rd Annual Conference of the IEEE Industrial Electronics Society*, pp. 5876–5881, Beijing, China, October 2017.

[17] M. Schwartz, F. Siebenrock, and S. Hohmann, "Model predictive control allocation of an over-actuated electric vehicle with single wheel actuators," *IFAC-Papers on Line*, vol. 52, no. 8, pp. 162–169, 2019.

[18] P. Dai and J. Katupitiya, "Force control for path following of a 4WS4WD vehicle by the integration of PSO and SMC," *Vehicle System Dynamics*, vol. 56, no. 11, pp. 1682–1716, 2018.

[19] P. Dai and J. Katupitiya, "Online path tracking and motion optimization of a 4WS4WD vehicle," in *Proceedings of the 2015 IEEE/RSJ International Conference on Intelligent Robots and Systems (IROS)*, pp. 4133–4139, IEEE, Beijing, China, September 2015.

[20] E. Ono, Y. Hattori, Y. Muragishi, and K. Koibuchi, "Vehicle dynamics integrated control for four-wheel-distributed steering and four-wheel-distributed traction/braking systems," *Vehicle System Dynamics*, vol. 44, no. 2, pp. 139–151, 2006.

[21] X. Zhang and V. Cocquempot, "fault tolerant control for an electric 4WD vehicle's path tracking with active fault diagnosis," *IFAC Proceedings Volumes*, vol. 47, no. 3, pp. 6728–6734, 2014.

[22] D.-Y. Li, Y.-D. Song, D. Huang, and H.-N. Chen, "Model-independent adaptive fault-tolerant output tracking control of 4WS4WD road vehicles," *IEEE Transactions on Intelligent Transportation Systems*, vol. 14, no. 1, pp. 169–179, 2013.

[23] A. Haddad, A. Aitouche, and V. Cocquempot, "fault tolerant control strategy for an overactuated autonomous vehicle path tracking," *IFAC Proceedings Volumes*, vol. 47, no. 3, pp. 8576–8582, 2014.

[24] F. Fahimi, "Full drive-by-wire dynamic control for four-wheel-steer all-wheel-drive vehicles," *Vehicle System Dynamics*, vol. 51, no. 3, pp. 360–376, 2013.